10

Adsorption of methane in porous materials as the basis for the storage of natural gas

Cecilia Solar, Andrés García Blanco, Andrea Vallone and Karim Sapag
Laboratorio de Sólidos Porosos-Instituto de Física Aplicada-CONICET, Dpto. de Física-Universidad Nacional de San Luis
San Luis, Argentina

1. Introduction

It is well known that the natural gas (NG) is a substance of fossil origin from the decomposition of organic matter. It is found trapped under the terrestrial surface in stratus that avoid the natural release to atmosphere. These underground deposits can be oceanic or terrestrial.
The NG is a homogeneous mixture, having variable proportions of hydrocarbons, being the main constitute the methane (CH_4), which content generally ranges from 55 to 98 % in volume. Also, it contains ethane (C_2H_6), propane (C_3H_8) and heavier constitutes. Although it can be found in gas phase or in solution with oil, under normal atmospheric conditions, remains in gas phase. It may have some impurities or substances that are not hydrocarbons, such as Hydrogen Sulfide, Nitrogen and Carbon Dioxide (Figure 1). According to its origin, natural gas is classified in *associated* and *non-associated*, being the first, the one which remains in contact and/or dissolved with the oil from the deposit. The non-associated gas can be found in deposits lacking oil crude at the initial conditions of pressure and temperature.

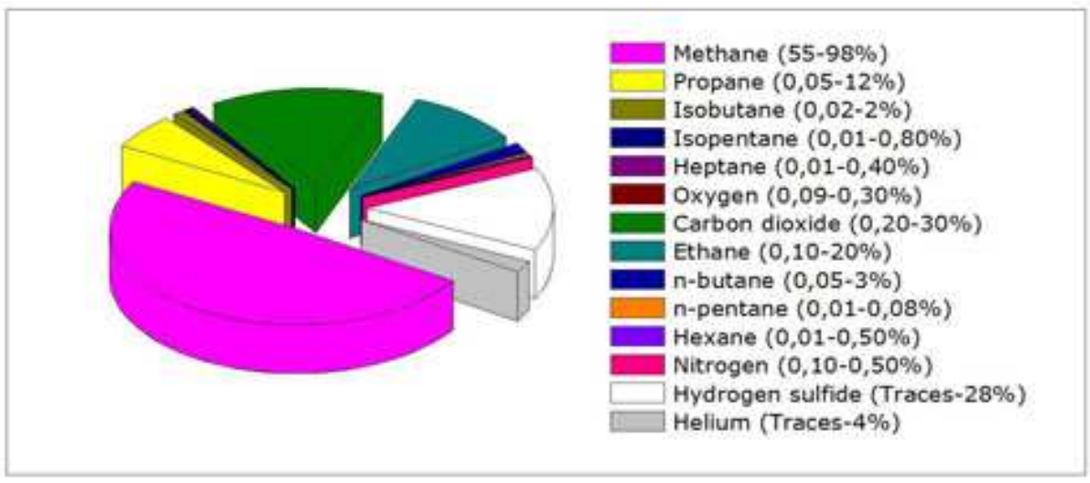

Fig. 1. Principal constitutes of Natural Gas (in percentage).

From the fossil fuels, the cleanest is the natural gas. Its combustion, similarly to other fuels, produces mainly CO_2 and water vapor. The emissions of CO_2 are 25-30% lower than the generated by the fuel-oil and a 40-50% lower than charcoal (Figure 2) per unit of produced energy (Natural Gas and Climate Change Policy, 1998; Comisión Nacional de Energía, 1999).

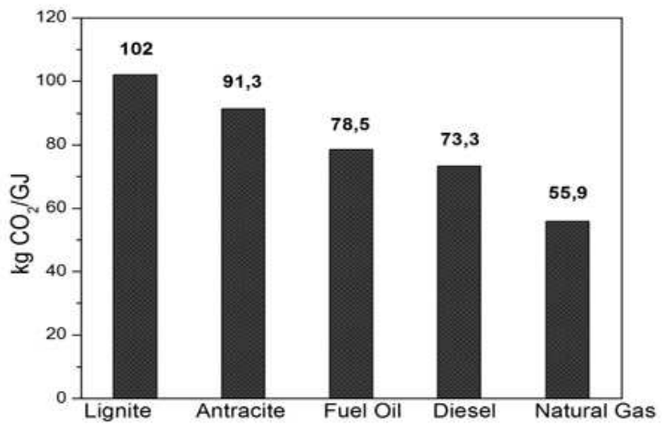

Fig. 2. CO_2 Emissions in the combustion (Kg per GJ).

At worldwide scale, the resources of natural gas are abundant. However, as oil, they are highly concentrated in a reduced number of countries and deposits. Some data reported in the *BP* Statistical Review of World Energy, 2009, revealed interesting information: three countries (Russia, Iran and Qatar), hold the 56% of the world reserves (WR). Almost the 50% of the WR are distributed in 25 deposits around the world and the countries that are members of the OPEC (Organization of the Petroleum Exporting Countries), control the 50% of the WR. The percentage distribution of the WR by the end of 2008 is shown in Figure 3.

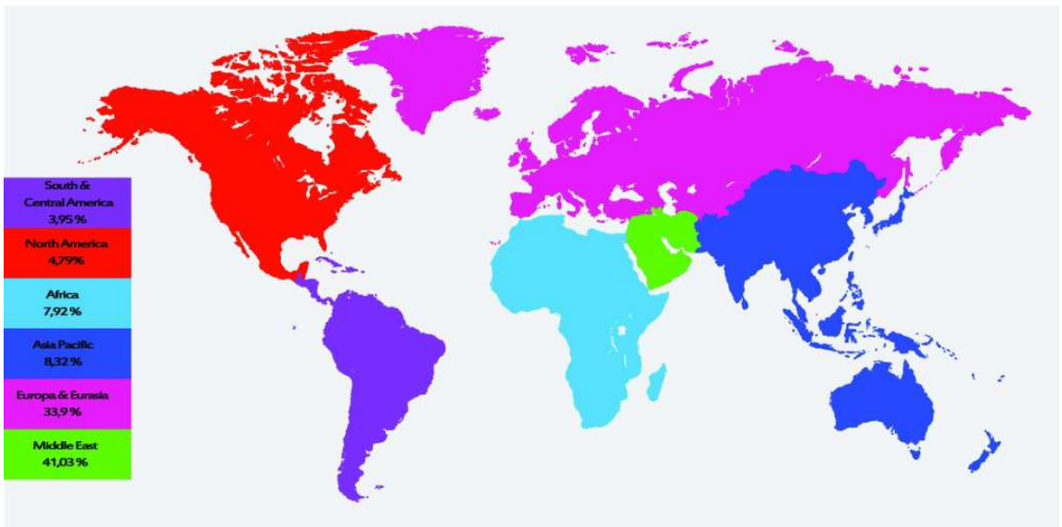

Fig. 3. The percentage distribution of the world reserves of natural gas by the end of 2008 according to the Statistical Review of World Energy, 2009.

As it may be seen from Figure 3, the world reserves of natural gas, although heterogeneously, are distributed throughout the world, constituting an advantage to be able to supply the local requirements. During the last few decades, the volume of discovered gas has been decreasing but it still keeps the necessary volume to ensure their existence for many years. Additionally, the estimations of these reserves are progressing as new techniques of exploitation, exploration and extraction, are discovered. It is estimated that a substantial quantity of natural gas remains undiscovered (World Energy Outlook, 2009).

The NG has vast diversity of applications: in industry, trade, energy generation, residential sector and terrestrial transport, and its use have shown an important growth over the last few years (MacDonald & Quinn, 1998; Inomata et al., 2002; Prauchner & Rodríguez-Reinoso, 2008).

Regarding the particular use as fuel for transport units, such as cars, autobuses and trucks, the natural gas vehicle (NGV) shows diverse environmental benefits. One of them is the reduction of post combustion contaminants, lowering the maintenance costs compared to traditional fuels (Cook et al., 1999; Lozano-Castelló et al., 2002a; Alcañiz-Monge et al., 1997).

The environmental advantages at using the NGV are numerous. However, from the point of view of the combustion products, it can be remarked: i) it does not contain lead or heavy metals traces, avoiding their emission to the atmosphere, ii) lack of suspended solid particles that are present when using gasoline affecting health (increase of respiratory and cardiovascular diseases), iii) absence of sulfur and subsequently no sulfur dioxide (SO_2) emissions, typical contaminant from transport. Compared to liquid fuels, the emissions of the NGV combustion produce up to 76% less CO, 75% less NOx, 88% less hydrocarbons and 30% less CO_2. Furthermore, the physicochemical properties of the natural gas enable the use of catalysts for the combustion of gases, obtaining excellent results and minimizing even more the emissions (Sun et al., 1997).

The advantages of NG have promoted its use in the automotive fleet of many countries, which exceeds six millions of vehicles at present. The advance in the technology for the NGV use has not been standardized throughout the world. This is due to differences regarding the availability of energy resources, contamination levels, fuel pricing policies, applied auditing and, definitely, the set of government actions able to generate expectative among the potential users.

Country	**Vehicles**
Pakistan	2,000.000
Argentine	1,678.000
Brazil	1,467.000
Italy	433,000
Colombia	251,000
India	225,000
EE.UU	130,200
Germany	54,200
Japan	24,700
France	8,400

Table 1. Estimated Natural Gas Vehicles in different countries.

Table 1 summarizes the number of natural gas vehicles in some representative countries according to the Dirección de Tecnología, Seguridad y Eficiencia Energética, 2006.

In spite of the advantages showed by the NG in comparison to liquid fuels, there is an important disadvantage: its low-energy density (heat of combustion/volume), which constitutes a limitation for some applications. Therefore, under standard conditions of pressure and temperature, the distance traveled by a vehicle per unit of fuel volume, using NG, corresponds to the 0.12% of the trajectory with gasoline. Consequently, the storage of this fuel, whether in quantity or density, plays an important role for its use in diverse kinds of transport.

An alternative is to increase the density, for example, liquefying the NG. The liquefied natural gas (LNG) is stored at the boiling point, 112K (-161ºC) in a cryogenic tank at a pressure of 0.1MPa, where the energy density is approximately a 72% of the total gasoline. This means that 1 volume of LNG corresponds to 600 volumes of natural gas under STP (600 v/v) conditions (Cracknell et al., 1993; Menon & Komarneni, 1998). However, this storage method shows multiple inconveniences, mainly because the LNG increases inevitably the temperature within the tank. Thus, the pressure rises and could result in a dangerous situation. Moreover, the filling of the tank must be performed by an expert on cryogenic liquids handling.

A widely used commercial method considered to increase the energy density of the natural gas is to compress and store it as compressed natural gas (CNG). For this case, the NG can be found as a supercritical fluid at room temperature and it becomes compressed at a maximum pressure around 20-25 MPa, reaching a density 230 times higher (230 v/v) than the one obtained for the natural gas under STP conditions (Menon & Komarneni, 1998; Lozano-Castelló et al., 2002b). In this case, the energy density is approximately 25% of the one from gasoline. A disadvantage is the risk of carrying highly compressed gas (20MPa) within the vehicle. Modifications such as thick-walled tanks and complex safety valves would be required.

The use of adsorbent materials, such as activated carbons and zeolites, among others (Rodriguez-Reinoso & Molina-Sabio, 1992; Parkyns & Quinn, 1995; Sircar et al., 1996; Alcañiz-Monge et al., 1997; Lozano-Castello et al., 2002c; Almansa et al., 2004; Marsh & Rodriguez-Reinoso, 2006; Mentasty et al., 1991; Triebe et al., 1996), for the storage of natural gas at low pressures, is known as adsorbed natural gas (ANG). Pressures are relatively low, of the order of 2 to 4 MPa at room temperature, which represents an interesting alternative for the transport and applications at large scale. The technology, in contrast with the other two, is not well developed and is still at scientific level. At this stage, the studies on storage by the ANG method are carried out using the methane, major constituent of the NG. It has been found that the density of the compressed methane at 3.4MPa can be increased in a factor higher than 4 by the use of adsorbents, reaching a relation of methane storage of 180 v/v, which is equivalent to compressed gas at more than 16MPa (Cook et al., 1999; Alcañiz-Monge et al., 1997).

Through this chapter, basic concepts regarding adsorption and adsorbents are reviewed as well as their application for the particular study of methane storage, starting point of the ANG process. In addition, the methodology for the study is described and shows the scientific advance in this field, reporting results from our research group and from other laboratories.

2. Adsorption basics and methodology of study

Adsorption is a phenomenon in which surface plays an important role, unlike absorption where molecules can penetrate the solid structure. The occurrence of this phenomenon in gas-solid interactions is our major focus of interest.

The surfaces of solids, even those homogeneous, have imperfections. These defects are the result of many circumstances, mainly its composition and the interaction that takes place among the molecules that constitute their atmosphere. Figure 4 shows a classical schema of this situation, according to the description made by Somorjai, 1994.

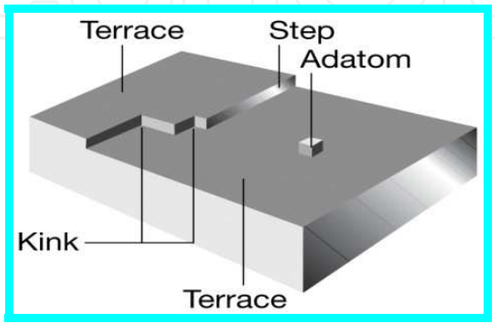

Fig. 4. Scheme of common defects on the apparently homogeneous solid surfaces.

Generally, the properties of the surfaces of the solids differ from their bulk for many reasons. Some of which are enlisted below:

- The perturbation of the superficial electron density is different to the one from the bulk. This is caused by the loss of structural periodicity in the perpendicular direction of the surface.
- The presence of decompensated forces on the surface due to the lack of neighbor atoms (producing potential wells, nearby molecules are attracted).
- Vibrational properties on the surface are different (geometrical and energetic effects, producing curvatures) from the ones on the rest of the solid.
- Some phenomena can occur: *Relaxation* or Superficial *Reconstruction*, which means that the superficial atoms show geometrical and energetic differences to the atoms from the bulk.

These reasons promote the presence of attractive potentials, which are able to attract molecules from the surrounding leaded by thermodynamic parameters, particularly, pressure P and temperature T of the gas-solid system. Moreover, superficial centers can take place showing additional electrostatic effects and creating new attractive or repulsive "sites". Therefore, when one or more molecules from a fluid approach the surface, they could be trapped and nucleation, motion and the formation of layers in the interface, would take place. This process is named Adsorption.

"Adsorption of a gas onto a solid surface" can be defined as the gain of one or more constituents of the gas in the region of the gas-solid interface. Figure 5 shows a schema that represents the process.

The adsorption phenomenon involves an increment of the gas density in the neighborhood of the contact surface and since the process is spontaneous, the change in the free energy of Gibbs is smaller than zero. Given that the entropy change is also below zero (a decrease in

the freedom degree of the gas molecules during the process), the enthalpy change is lower than zero. Thus, the process is exothermic (Rouquerol et al., 1999).

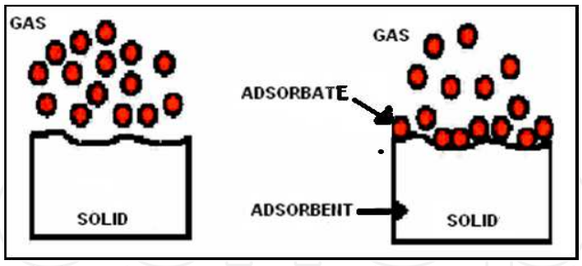

Fig. 5. Representation of the adsorption process of a gas on a solid surface for a given pressure, P and temperature, T.

When the adsorption process is reversible it means physical adsorption or physisorption, our major focus of interest for the study of natural gas storage. In this case, the result of the adsorption heats or enthalpy changes in the process are not elevated values, being for the methane about 16 KJoule/mol (Cook et al., 1999). The interaction forces occurring between the solid surface (adsorbent) and the adsorbed gas (adsorbate) are Van der Waals type, where prior to adsorption, the gas is called adsorbable. Moreover, adsorbate-adsorbate interaction may take place and is neglected in some studies when compared to the adsorbate-adsorbent interaction. It can also be considered that in average, these interactions do not impact the whole process.

The net interaction potential that the molecules surrounding the surface may experience, can be represented as seen in Figure 6, where the energy of interaction of one particle at a distance z of the surface, is the sum of the interaction of each molecule(i) with each atom (j) of the solid, given by equation 1.

$$E(z) = \sum_{j} \phi_{ij} \tag{1}$$

Figure 6 represents a particle with a kinetic energy E_k approaching to the solid surface.

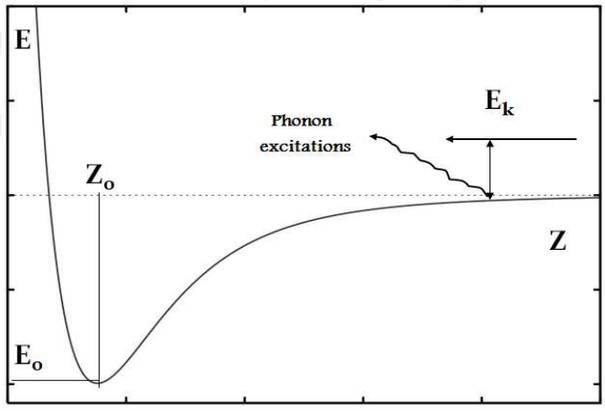

Fig. 6. Representation of the interaction potential that molecules nearby to the surface may sense.

The particle may detect the phonons excitation and subsequently, the potential attraction of the solid, which has a minimum (value) at a distance Z_0, representing the minimal distance of approaching to the solid.
The energy of the adsorbate-adsorbent interaction can be expressed using several terms. Some of them are described in the following equation:

$$E(z) = E_D + E_R + E_P + E_{dip} + E_Q \quad (2)$$

where E_D represents the dispersive potential (attractive); E_R, the repulsive; E_P, the one caused by the polarizability; E_{dip}, the dipolar and E_Q, the quadrupolar interactions (Rouquerol et al., 1999).
Considering only the first two terms, a Lennard-Jones (L-J) potential would take place, which involve the Van der Waals attractive forces and the Pauli repulsive forces.

2.1 Quantification of the Adsorption

Assuming a system set at a given temperature where a gas becomes into contact with a solid surface occupying a volume V at a pressure P_i prior to the adsorption, while a part of the adsorbable gas passes to the adsorbed state, keeping V and T unchanged, it should be noted a pressure decrease, followed by a stabilization of the system to a final equilibrium at pressure P_{eq}. Figure 7 represents the adsorption process at constant V and T.

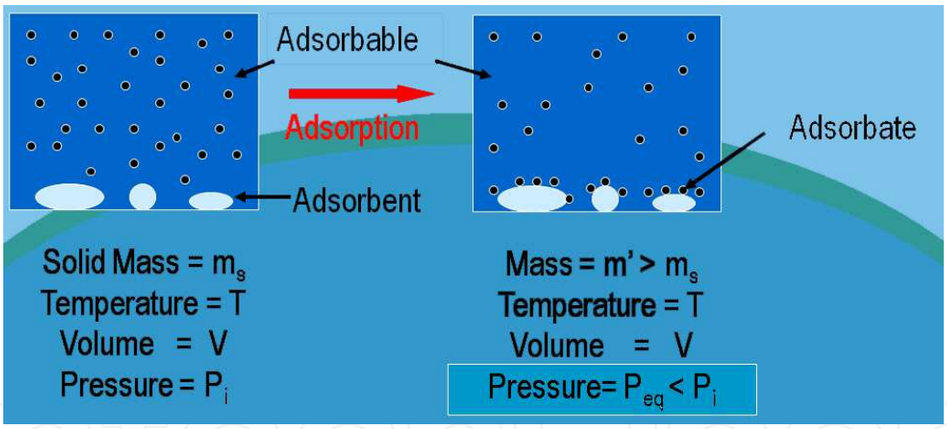

Fig. 7. Scheme of the Adsorption process.

Once the pressure change (P_i-P_{eq}) is determined by an equation of state that represents the gases under study, it is possible to calculate the quantity of moles that are no longer in gas phase but in the adsorbed phase at that pressure. The same can also be expressed in terms of adsorbed volume or grams of adsorbate, which is usually reported in standard conditions of temperature and pressure. Whether P_i is increased, a new P_{eq} is obtained as well as a new adsorbed quantity, maintaining unchanged the temperature and volume of the system. Thereby, the relation between the adsorbed amount and the pressure may be graphically found at constant temperature, reported as *adsorption isotherm*. This method, called volumetric or manometric, is the most widely used to measure the adsorption of gases and was selected for our laboratory to study adsorption processes. By the gravimetric method, the adsorbed quantity is measured from the mass gain during the process.

There is a detail that must be appointed because it would be helpful when interpreting what it is being actually measured. Assuming than n moles of an adsorbable are put into contact with a solid (adsorbent) at a certain volume V and pressure P where the adsorption occurs, once the equilibrium is reached, it is possible to identify three zones with different concentrations $c = dn/dV$, as shown in Figure 8a. Zone I corresponds to the region where the adsorbent is located and none molecule of adsorbable is expected ($c^s=0$). Zone II corresponds to the adsorbed layer, focus of our interest, where the concentration is c^a, which decreases as z increases ($c^a=c(z)$) until $z=t$. The zone III is at c^g concentration, which is the concentration of the adsorbable in absence of the adsorbent and depends only on P and T.
Knowing the area A, where the adsorbed layer is on the surface, as well as the thickness of the adsorbed layer t, the volume of the adsorbed layer can be calculated as $V^a=A.t$, from where the adsorbed quantity in moles, can be deduced.

$$n^a = \int_0^{V^a} c^a dV = A\int_0^t c^a dz \tag{3}$$

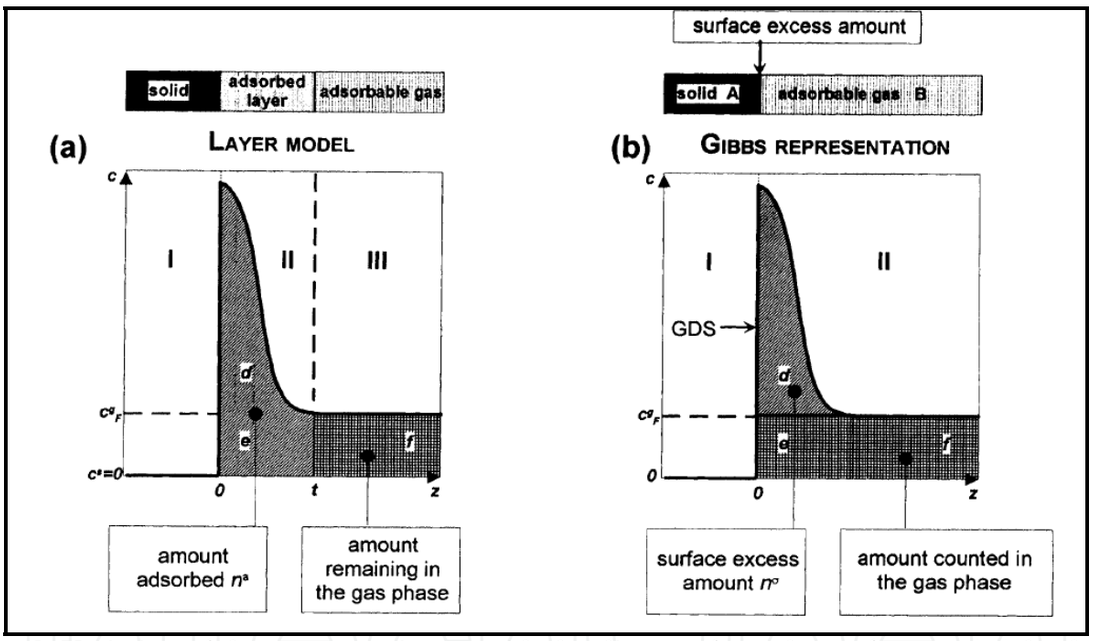

Fig. 8. Variation of the concentration, c, with the distance from the surface, z. a) Adsorbed layer; b) Gibbs representation (from Rouquerol et al., 1999).

The total quantity of moles for the considered volume is:

$$n = n^a + c^g V^g \tag{4}$$

where V^g is the gas volume that remains at zone III (f region indicated in Fig 8a) after the adsorption process.
Therefore, in order to calculate n^a it must be known the c^a as z function (eq. 3) or V^g and n from eq. 4. However, the concentration profile of the adsorbed zone cannot be determined through an assay, and a measure of the volume V^g is complicated to obtain. This is because when adsorption occurs, the decrease in the system pressure is due to the increase in the

molecules concentration (zone *d* of Figure 8a) at concentrations higher than c^g. On the other hand, the molecules of the zone *e* are at the same concentration than the adsorbable and do not causes a pressure decrease. This would complicate the identification of the molecules that are in the zone *e* and *f*, occupying these latter the volume V^g.

To overcome this inconvenient, the Gibbs representation (Figure 8b) can be used. In this case, the system of reference occupies the same volume than the actual but, at present, it is only divided in two regions: I, the solid and II, the zone where the adsorbable is located. The status of the adsorbable remains unknown (adsorbed or not), while it is separated by a surface that is parallel to the adsorbent, called Gibbs dividing surface (GDS). The actual volume occupies the same volume than the representation, *V*, which is the volume that the molecules (*n*) occupy when put into contact with the solid at an initial pressure P_i. Afterwards, when the equilibrium is reached, a P_{eq} value arises. The entire process follows Figure 7.

Zone II of Figure 8b is the resulting scenario when P_{eq} is reached. Then, the gas molecules can be taken as part of one of two groups: the molecules that maintain the concentration of the gas, c^g, simulating that the adsorption phenomenon does not occur (zones *e* and *f* of Figure 8b), and another group that includes the molecules showing a concentration higher than c^g, that are basically, "*excess*" molecules (zone *e*) called n^σ. These are responsible for the decrease of P_i and the unique measurable molecules in an assay.

In conclusion, the number of "*excess*" molecules is the difference between the total number of molecules and the number of molecules remaining at the same concentration of the gas prior to be adsorbed:

$$n^\sigma = n - c^g V \tag{5}$$

Combining both schematic representations shown in Figure 8, it can be seen that the total volume is the sum of the volume V^g (zone III, Figure 8a) and V^a (zone II Figure 8a). This could be summarized as follows:

$$n^\sigma = n - c^g V^g - c^g V^a \tag{6}$$

From equation 4, it can be obtained the number of molecules from the adsorbed layer (n^a) as a function of the number of total molecules of the studied gas (*n*). Correlating eq. 4 and 6, we obtain:

$$n^a = n^\sigma + c^g V^a \tag{7}$$

At a low pressure assay, c^g corresponds to a small value and $V^a << V^g$. Hence, from equations 6 and 7, we find that:

$$n^a \approx n^\sigma \tag{8}$$

This does not occur at high pressures (pressures higher than the atmospheric), where eq. 7 remains valid.

It can be concluded that the measures that actually can be performed in an assay, are the molecules present in the "*excess*" zone, shown in the Gibbs schema. Therefore, the experimental data that can be graphed correspond to an *excess isotherm*, given by the n^σ molecules. Sometimes the interest is focused on the *absolute isotherm*, particularly for

comparison with theoretical calculations and it is obtained by counting n^a. To conduct assays at subatmospherical pressure, these two isotherms are coincident, but it is not valid for high pressures.
The major interest in this chapter is to use these concepts to achieve adsorption isotherms of methane at low and high pressures. Afterwards, it is possible to obtain information regarding the possibilities of natural gas storage with the adsorbents under study.

2.2 Porous materials

Adsorption is a superficial process and a crucial characteristic for the adsorbents is their high adsorption capacities. Then, the adsorbents require an elevated exposed surface per gram of material, which is called *specific surface area* (S_{esp}) and is expressed in cubical centimeters of adsorbate per gram of adsorbent.
The smaller the elemental constituents of the solid are, the greater the specific surface area is. This characteristic may be shown in fine particles, e.g. powders, as well as solids with small holes, which sizes can range from a few Angstroms to nanometers. These are named *porous solids*.
The IUPAC (Sing et al., 1985), depending on the transversal dimension of the pores in these solids (d), present the following classification:

$$solids \begin{cases} micropores\ d < 20\,\text{Å} \\ mesopores\ 20\,\text{Å} < d < 500\,\text{Å} \\ macropores\ d > 500\,\text{Å} \end{cases}$$

A solid may exhibit different kinds of pores. Rouquerol et al., 1994 reports diverse possibilities (Figure 9) where the contribution to the specific surface area is variable. The more rough the surface is or the smaller the pores are the greater is the contribution to the S_{esp}.

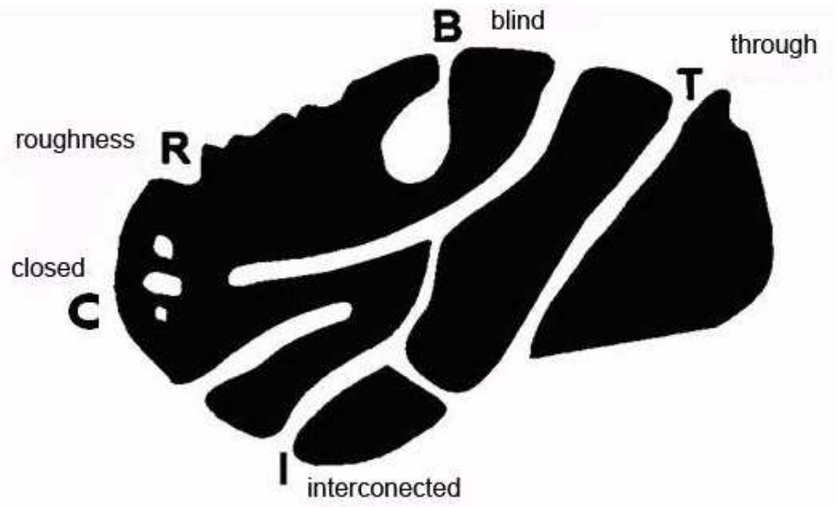

Fig. 9. Types of pores that a solid may exhibit Rouquerol et al., 1994.

Up to present, the adsorption phenomenon has only been studied from the perspective of a plane solid surface and a gas. However, for porous solids the gas molecules are *"surrounded"* by the walls of the pores, being considerably higher the interaction forces. In order to model this interaction, it must be supposed that the potential of the walls has an attractive and a repulsive term, similar to the aforementioned potential style described by Lennard Jones (Figure 6). As the pore becomes smaller, the potentials of the gas-solid interaction of each wall overlap. This, results in further potentiation of the adsorption phenomenon, which turns porous materials into excellent adsorbents. Figure 10 shows a schema of the variation of the potential of the solid-gas interaction for a plane surface and a porous solid while the separation among layers, decreases.

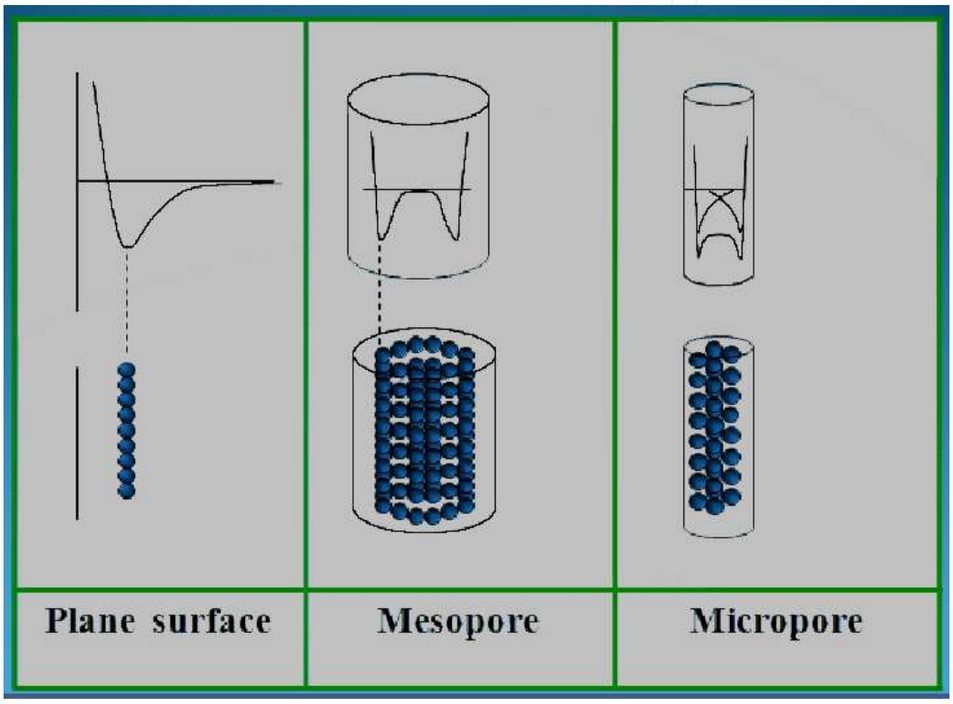

Fig. 10. Potential configuration according to the surface.

Therefore, besides the specific surface, it becomes necessary to study the porosity of the sample to provide comprehensive information related to the adsorption capacity.

2.3 Gas adsorption for the characterization of materials

The textural characteristics of the solids can be studied by gas adsorption, usually with gaseous nitrogen at 77K, at pressures between 10^{-4} Torr to pressures near to the atmospheric. As a result, adsorption isotherms may be obtained and reflect the quantity of adsorbed gas (cm^3/g) as a function of the relative pressure (P/P_0) at constant temperature, where P_0 is the saturation pressure. The appearance of the isotherm is directly related to the characteristics of the solid. An extensive work conducted by Brunauer, Deming, Deming and Teller (Brunauer et al., 1940), reported that a isotherm can be described by one or a combination of the basic shapes illustrated in Figure 11.

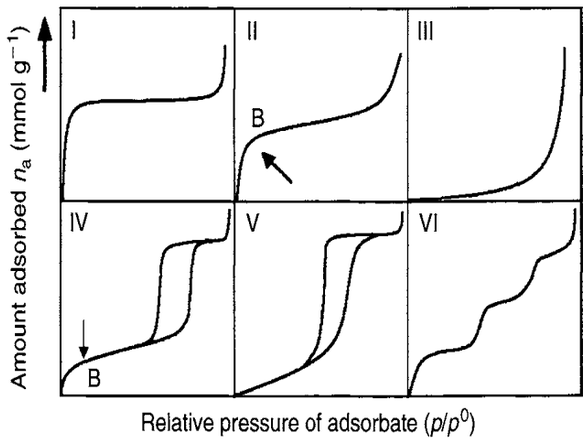

Fig. 11. Types of isotherms representing the most relevant processes taking place in the adsorbate-adsorbent interaction (from Rouquerol et al., 1999).

It should be noted that the shape of the isotherms reveals the diverse processes than can occur as the pressure increases. At low pressures, micropores become filled and a monolayer reaches its capacity at relative pressures of the order of 0.1. From that point, a mono-multilayer filling begins and a capillary condensation is produced at pressures of the order of 0.5 of P/P_0. Afterwards, the mesopores become filled and at pressures near to P_0, the condensation of the N_2 takes place (for N_2 isotherms at 77K). This technique is useful to analyze up to mesopores.

For the storage of methane, the materials of interest must have micropores that show Type I isotherms at the zone of low pressures. However, at high pressures, these materials can have a mono-multilayer filling, typical of mesopores, and hysteresis loops, related to the pore geometry.

From the measured isotherms (Vads vs P/P_0), it is possible to obtain some textural characteristics of the material, such as specific surface area, pores volume, micropores volume, etc. For that purpose are used models that assume the form of the pores and their way of filling, as well as the gases state.

In regards to the models and the manner in which data are obtained for further characterization, notable works have been reported (Gregg & Sing, 1982; Rouquerol et al., 1999).

For the calculation of the specific surface of the solids, the most used method is the one proposed by Brunauer, Emmet and Teller, the BET method (Brunauer et al., 1938). Starting from the thermodynamic equilibrium, at a determined pressure P and temperature T, a series of assumptions are made regarding the events that occur in the gas-solid interface, where molecules reach towards the surfaces. Some of the remarkable assumptions are:

-That the adsorbed molecules are spherical-shaped and gradually accumulate on the surface of the solid. Whether they group side by side, they can form a monolayer.

-That regions exist on the surface of the solid and are covered with 0, 1, 2… m monolayers of molecules.

-That the adsorption energy is E for the first layer and E´ for any other layer and lateral adsorbate-adsorbate interactions do not exist.

-That at equilibrium, the quantity of molecules that enter and exit is the same at a determined region.

From these assumptions, and attending to the kinetic-molecular theory of gases, the following isotherm, known as BET equation, is obtained:

$$\frac{P/P_0}{n_a(1-P/P_0)} = \frac{1}{n_m C} + \frac{C-1}{n_m C}(P/P_0) \tag{9}$$

where P/P_0 is the relative pressure, n_a is the number of adsorbed moles, n_m is the number of moles per gram of solid within a monolayer, and C is a constant related to the energy of adsorbate-adsorbent interaction.

Equation 9 represents the equation of a straight line with slope $\alpha = \frac{C-1}{n_m C}$ and ordinate to the origin $\Omega = \frac{1}{n_m C}$, where n_m and C, may be obtained.

From n_m (mol/g) and having the surface that the gas spheres occupy, A_m *(m²/molecule)*, and the number of molecules that occupy a mol N (*molecules/mol*), it can be stated:

$$S_{BET} = n_m . A_m . N \tag{10}$$

in m²/g, which represent the specific surface area by the BET method (S_{BET}).

Although this method makes basic suppositions and perhaps unrealistic, it is still a simple method widely used and standardized for the calculation of the "BET specific surface area" *(S_{BET})*. This method is effective for materials with mono-multilayer formation, particularly when the monolayer is well-formed. This is the case of the type II isotherms from Figure 11, where B points out the zone where the monolayer becomes filled. For microporous materials, caution is necessary because S_{BET} usually overestimates the value of the specific surface area. Rouquerol et al., 1999 detail a series of conditions that must be fulfilled in order to obtain the most accurate calculation.

There are various methods available to calculate the microporosity. One of the most used and accepted is the proposed by Dubinin and collaborators (Dubinin, 1960), which is based on Polanyi's theory, that supposes the existence of adsorption potentials, characteristic of the adsorbents. The adsorbed quantities are a function of this potential and constitute the "characteristic curves". Based on this theory and studying diverse adsorbates on the same surface, Dubinin found that characteristic curves were affined, differing in one constant and with a similar shape to the "tail" of a Gaussian. Hence, he suggested a general shape for these curves and using the Polanyi potential, proposed to calculate special characteristics of the material, particularly the micropores volume. These calculations were performed at the region of low relative pressures, where the process involved in the adsorption is the micropores filling instead of the layer-by-layer adsorption on the pore walls. The following relation, named Dubinin-Raduschevich (Rouquerol et al., 1999), was found:

$$\log(V) = \log(V_o) - D.\log^2\left(\frac{P_o}{P}\right) \tag{11}$$

where V is the adsorbed volume, V_0 is the micropore volume and D is related to the pore size and involves the assay temperature and the affinity of the used adsorbate. The data obtained from the isotherm can be used to determine the micropore volume by the ordinate to the origin, graphing the implicit linear equation (eq. 10).
In consequence two fundamental determinations regarding the characterization of a porous material are S_{BET} and its V_o.
The N_2 at 77K is widely used for the characterization of porous materials. However, for narrowed micropores often called ultramicropores (< 8 Å), this gas has shown diffusion problems. For this reason, CO_2 has been proposed as an alternative characterization gas in this porous region. Since results have been satisfactory (Garrido et al., 1987), studies reporting microporous characterization using CO_2 has become common.
Additionally to experimental data, computational studies are often made in order to obtain information regarding the texture of the materials.

2.4 Computational studies for adsorption

2.4.1 DFT Method

A widely used methodology for the calculation of the pore size distribution is based on the Density Functional Theory, DFT, (Latoskie et al., 1993; Neimark et al., 1997; Neimark et al., 2000; Tarazona, 1985; Murata et al., 2000), which is already incorporated to the software in several equipments. A brief description is given below.
The thermodynamic system chosen to apply the DFT methodology in the adsorption of porous solids is the macrocanonical ensemble. The potential in this ensemble (grand potential) is given by $\Omega(\rho(r))$, which at equilibrium is defined as follows:

$$\Omega(\rho(r)) = A(\rho(r)) + \int dr\rho(r)\left(V_{ext} - \mu\right) \tag{12}$$

where $A(\rho(r))$ is the free energy, $\rho(r)$ the density profile, V_{ext} is the wall potential and μ the chemical potential.
The equilibrium density profile is therefore determined by minimizing the grand potential functional with respect to **ρ(r)**. Since ρ(r) is the local density, the adsorbed amount (usually expressed as the surface excess number of adsorbed molecules) must be obtained by the integration over the internal volume of the pore. By repeating this procedure with different values of μ (and hence values of P/P_0) it is possible to construct the adsorption isotherm.
The evaluation of the excess free energy is a more difficult problem. This is because in an inhomogeneous fluid the energy distribution is non-local; it depends on the correlations within the overall density profile. Various attempts have been made to overcome this difficulty by the introduction of weighting or smoothing functions (Gubbins, 1997). This approach has led to the development of the non-local density functional theory (NLDFT), which inter alia has been used for the derivation of the pore size distribution from adsorption isotherm data.

2.4.2 Monte Carlo Method

According to statistical thermodynamics, a system where the chemical potential μ, volume V and temperature T, remain constant while energy and particles are exchanged with the reservoir, is called Grand Canonical ensemble. This kind of ensemble is appropriate for describing an adsorption process of a liquid or a gas on solid surfaces.

Framed in the formal terms characterizing the present ensemble, the Grand Partition Function is set out, from which it is possible to obtain relevant thermodynamic parameters, given in equation 13 (Hill, 1986).

$$\Xi = \sum_{N} \frac{\lambda^{N}}{N!\Lambda^{3N}} \int \exp\left(-\beta U_{N}\right) dr^{N} \tag{13}$$

where U_N is the total energy of the system, $\lambda = \exp(\beta\mu)$ and $\beta = 1/k_B T$. The probability to find the system at a state i with N molecules in a volume element of the phase spaces; $\delta\vec{r}^{N}\delta p^{N} = \delta\vec{r}_1 \ldots \delta\vec{r}_N \delta\vec{p}_1 \ldots \delta\vec{p}_N$ is $f_i \delta\vec{r}^{N}\delta p^{N}$, where:

$$f_i \propto \frac{(\xi V)^{N}}{N!} \exp\left(-\beta U_{N}\right) \tag{14}$$

being $\xi = \frac{\lambda}{\Lambda^3}$ the affinity (for an ideal gas, $\xi = P/k_B T$)

Once the thermodynamic relations of the system are established, the simulated adsorption isotherms can be obtained by studying the situation of the molecules approaching to the surface.

Three elemental processes keeping T and μ unchanged can be considered: Adsorption of a molecule, desorption and displacement (defined as the sum of the desorption and re-adsorption of the same molecule). Using equation 13 and an algorithm, such as the proposed by Metrópolis (Frenkel & Smit, 2002) to calculate the probabilities of transition from an initial state to a final state, it can be obtained:

$$a).\ Displacement: \quad p_{ij} = \min\left\{1, \exp\left[-\beta\left(U_N(i) - U_N(j)\right)\right]\right\} \tag{15}$$

$$b).\ Adsorption: \quad p_{ij} = \min\left\{1, \frac{\xi V}{N+1}\exp\left[-\beta\left(U_{N+1} - U_N\right)\right]\right\} \tag{16}$$

$$c).\ Desorption: \quad p_{ij} = \min\left\{1, \frac{N}{\xi V}\exp\left[-\beta\left(U_{N-1} - U_N\right)\right]\right\} \tag{17}$$

One Monte Carlo step consists on choosing one of the three mentioned processes, assuring equal probabilities. In each case, the displacement, adsorption or desorption for every randomly chosen molecule is performed as described in previous reports (Nicholson & Parsonaje, 1982; Frenkel & Smit, 2002; Sweatman & Quirke, 2006). This process is carried out a sufficient number of times (of the order of $2x10^7$ Monte Carlo steps) and the average of N

(number of molecules) and U (internal energy) is determined. Subsequently, another μ value (or P value) is set and an adequate number of Monte Carlo steps are performed to reach the N and U average values. Thereby, the quantity of adsorbed molecules is calculated as a function of P (or μ), which is precisely, the adsorption isotherm.

The pressure within the reservoir is related to the chemical potential through:

$$\beta\mu = \beta\mu^{\theta}_{id\ gas} + \ln\left(\beta P_{id\ gas}\right) \tag{18}$$

Whether the work pressure is high enough, the ideal gases equation is no longer valid and a state equation must be used to correlate the chemical potential of the reservoir with the pressure.

$$\beta\mu = \beta\mu^{\theta}_{id\ gas} + \ln\left(\beta P\phi\right) \tag{19}$$

where ϕ is the coefficient of fluid fugacity within the reservoir. In order to calculate ϕ, the state equation is used, i.e. Peng-Robinson (Frenkel & Smit, 2002).

2.4.3 Interaction potentials

To perform a simulation of a gas-solid adsorption process, the interaction potentials gas-gas and gas-solid must be taken into account.

Most methods used for molecular simulation consider gases as interaction sites among the centers of the molecules via Lennard-Jones potential. However, this approximation may be enhanced.

For the calculation of the total energy of the system U, it must be considered the interaction potential among adsorbate molecules (Ugg) and between the adsorbent walls and the adsorbate molecules (Ugs).

The interaction potential among adsorbate molecules is given by the Lennard-Jones potential:

$$U_{gg}(r) = -4\varepsilon_{gg}\left\{\left(\frac{\sigma_{gg}}{r}\right)^{6} - \left(\frac{\sigma_{gg}}{r}\right)^{12}\right\} \tag{20}$$

Where ε_{gg} and σ_{gg} are the energetic parameters of the L-J potential and r is the separation among the molecules. The calculation of this potential is subjected to a cut-off distance beyond which, it is assumed that the Ugg potential is zero ($6\sigma_{gg}$ is usually taken).

In order to calculate the gas-solid potential, Ugs, some aspects must be taken into account such as the chemical composition of the solid surface and more importantly, the pore shape, especially if the pores are small.

For the slit-shaped pores, like two parallel graphite layers as illustrated in Figure 12, the potential proposed by Steele (Steele, 1974) may be applied. The following expression corresponds to this potential to calculate the interaction between an L-J site of an adsorbate molecule i, and the graphite layer of the surface, s:

$$U_{i_a s}(z_{i_a}) = 2\pi\varepsilon_{is}\rho_c\sigma_{is}^2\Delta\left\{\frac{2}{5}\left(\frac{\sigma_{is}}{z_{i_a}}\right)^{10} - \left(\frac{\sigma_{is}}{z_{i_a}}\right)^{4} - \frac{\sigma_{is}^4}{3\Delta\left(z_{i_a}+0.61\Delta\right)^3}\right\} \quad (21)$$

Where ρ_c is the density of interaction centers within the pore wall and Δ is the separation between the graphite layers of the pore wall. For graphite, ρ_c=114 nm^{-3} and Δ=0.335 nm and z represents the distance between the mass center of the adsorbate molecule and the centers of the carbon atoms from the first layer of the surface.

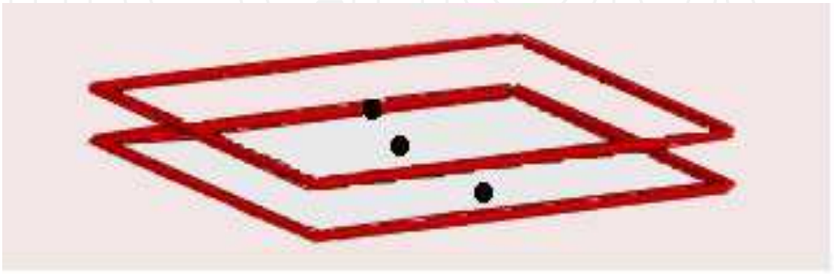

Fig. 12. Geometry of the pore showing parallel layers configuration, widely used to represent activated carbons.

Figure 13 illustrates an example of the interaction potential behavior between a pore wall (graphite) and a CH_4 molecule as a function of the separation distance from the z centers.

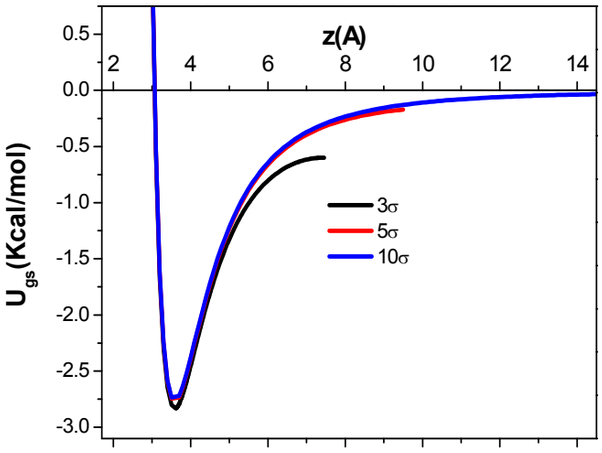

Fig. 13. Gas-solid interaction potential for a graphite layer and a CH_4 molecule for three pore sizes: $3\sigma_{gg}$, $5\sigma_{gg}$ and 10 σ_{gg}.

2.4.4 Characterization – Determination of the pore size distribution

The pore size distribution (PSD) of a porous material is one of the most crucial properties to predict the expected behavior for that material. This is particularly important because the

application of the material (gas separation, gas storage, pollutant adsorption, etc.) is based on this characteristic.

The determination of the pore size of non-crystalline materials, such as the activated carbon, is not an easy task considering that materials showing a crystalline arrange, such as zeolites, require a simple DRX analysis to accurately determine the pore size. Gas adsorption probably constitutes the most used tool for PSD calculation and at this point, molecular simulation has played a relevant role during the last few years.

To obtain the PSD, the solution of the generalized equation of adsorption is required:

$$V(P) = A\int f(w)v(w,P)dw \tag{22}$$

where *V(P)* corresponds to the experimental isotherm (volume of excess adsorbate under STP per gram of adsorbent), *f*(w) is the pore size distribution and *v*(w,P) is the average density (in excess) of adsorbate in a pore with size w, obtained by simulation.

Equation 22 is a Fredholm integral equation of the first type and its solution does not constitute a simple problem. Therefore, various methodologies of resolution are known for this equation, among which are remarkable the best fit and matricial methods. In any case, the introduction of regularization parameters is necessary to ensure a "more physical" meaning for the calculated PSD (Sweatman & Quirke, 2006).

The study of the characterization methods for porous materials, in particular by PSD, is an active field, supported by numerous reports. For activated carbons (AC), besides the slit-shape pores, other geometries have been studied, like the squared, rectangular (Davies & Seaton, 1998; Davies & Seaton, 1999, Davies et al., 1999) or triangular (Azevedo et al., 2010) geometries as well as the introduction of heterogeneities on the surface of the graphite layers (Lucena et al., 2010). In general, these approximations are improvements regarding the simulated isotherm fitting and constitute an example of the vast number of factors that have to be considered when simulating the adsorption of this kind of materials.

Another study field is the PSD calculation from the adsorption isotherms obtained for diverse gases, having different sizes and thermodynamic conditions (below or above the Tc) (Quirke & Tennison, 1996; Samios et al., 1997; Ravikovitch et al., 2000; Scaife et al., 2000; Sweatman & Quike, 2001a; Sweatman & Quike, 2001b; Jagiello & Thommes, 2004; Jagiello et al., 2007; Konstantakou et al., 2007; García Blanco et al., 2010). Results have shown discrepancies among the obtained PSDs and have evidenced the convenience of using gases as CO_2 and H_2 for the characterization of materials exhibiting ultramicropores (smaller than 0.7 nm). The N_2 at 77K has shown diffusion limitations at this region but is quite useful for pores with higher sizes, such as the mesopores (50 nm). Therefore, it seems to be clear that a special gas that characterizes with absolute accuracy does not exist. However, several gases can be used in order to obtain an adequate characterization. The characterization of the material under the habitual conditions in which it would be employed can be even more important, for example in the study of the methane storage.

Revealing information has been obtained through simulation techniques regarding the pores required for the storage of methane. For instance, Cracknell et al. 1993 reported a study from a Grand Canonical Monte Carlo (GCMC) simulation, where they compared the methane adsorption on AC with pores showing diverse geometries. It was found that the AC that shows the geometry of parallel plane layers, is also the one that posses the highest

adsorption capacity: 166 g/L at 274 K at 34 bar contrasting with results obtained for the zeolites-type geometry, 53.1 g/L, under the same conditions. Additionally, an optimal size of 3 σ_{gg} was reported by Tan & Gubbins, 1990 from data of GCMC and NLDFT simulations. It was concluded that the pore size that maximizes the adsorption of methane falls between 2.9σ_{gg} and 3.9 σ_{gg} (1.1-1.4 nm). Matranga et al., 1992 determined a size of 1.14 nm for a pore showing parallel plane layers configuration intended for a storage system at 34 bar.

2.4.5 Density of the adsorbed phase of methane

As it has been mentioned, the methane overcomes its critical temperature at room temperature and therefore, it should be impossible to condensate under isothermal conditions. This implies that the phase cannot be assumed to remain in liquid phase under these conditions, as occurs for the adsorption of vapors. Consequently, the state of an adsorbed phase for supercritical gases is an unclear subject and for that reason, there are diverse approximates for the calculation of the density or volume of the adsorbed phase (Murata et al., 2001; Zhou et al., 2001; Do & Do, 2003).

Previous studies have reported that the adsorption of supercritical gases tends to accumulate the adsorbate molecules in the neighborhood of the adsorbent surface. Also, it has been observed that a monolayer is usually formed to the distance from the wall that matches the minimum value of the curve of gas-solid potential. This means that only the micropores having sizes of a few molecular diameters are "full" of adsorbate, while higher micropores and mesopores have an adsorbed phase of one or two molecular diameters. This has important consequences on the study of the adsorbed natural gas and agrees with the pore sizes proposed by the bibliography.

Figure 14 illustrates the density profiles of molecules adsorbed into the pore obtained by Monte Carlo simulation. In small pore sizes (3σ_{gg}), there is a vast quantity of molecules distributed into the pore but, as the pore size increases, it can be seen at most, the adsorbed phase composed by a layer of two molecular diameters of thickness. At a pressure of 35 bar, no adsorbed phase was detected in the center of a 7σgg (2.6 nm) pore, instead, the density profile matches the density of the gas at this pressure.

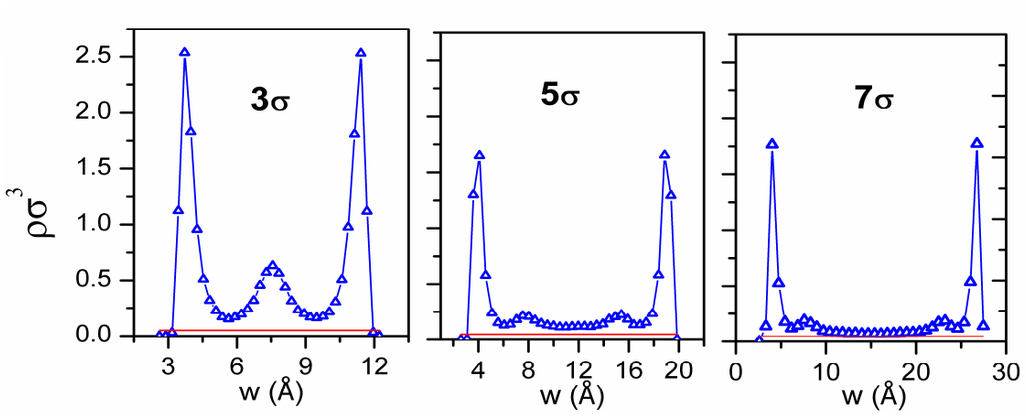

Fig. 14. Density profiles for methane molecules in slit shaped pores with different widths (3,5,7σ_{gg}) at 35 bar obtained from GCMC (Figure supplied by A. de Oliveira, INFAP-CONICET).

3. Adsorbents for the ANG process

Various studies have concluded that the features required by an adsorbent to be adequate for the ANG process are:

a) High adsorption capacity.
b) High adsorption/desorption relations.
c) Micropore sizes of approximate 0.8 nm (bigger than the sizes of two molecules of methane) to facilitate the gas release at room temperature.
d) High packaging density to ensure that the storage capacity and the energetic density are high.
e) Low adsorption heat and high specific heat to minimize the temperature variation in the tank through the adsorption and desorption processes.
f) Suitable properties for the mass transference.
g) Being extremely hydrophobic.
h) Being inexpensive.

To evaluate the quality of the adsorbent for being used in the ANG process for vehicles, there is a parameter called "delivery". It is defined as the gas delivered per unit of stored gas and is expressed by V/V. Specifically delivery is the quantity of gas released from the adsorbent when pressure is reduced to the atmospheric pressure.
During the 90s, the United States Department of Energy of the (USDOE) established an objective of 150 v/v of delivery in vehicles having ANG working at a pressure of 3.5 MPa at 25^{o}C (Cook et al., 1999).
In general, the adsorbent has a porous structure where the molecules that pass through it, can be retained (adsorbed) due to the high affinity that exhibit towards the adsorbent. These adsorbed molecules have a higher density than the one showed at the gas phase.
The suitable adsorbent to be used in the ANG process must be predominantly microporous. Therefore, the storage capacity is optimal when the volume fraction of the deposit corresponding to the micropores, is maximum. Besides, certain contribution of mesoporosity with a size smaller than 5 nm is, to some extent, required to yield the circulation of methane to the micropores interior.

4. Results from our research group

The final section of this chapter presents some of the results obtained in our laboratory regarding ANG studies.

4.1 Powdered activated carbons

In the first place, are shown results using activated carbons (AC) obtained from inexpensive materials as agricultural residues produced by the regional industry. ACs are synthesized by two procedures:
-Chemical activation, using an activating agent such as zinc chloride ($ZnCl_2$).
-Physical activation, using water vapor as activating agent.

Olive and grape lexes were used as precursors. The term lex is used to designate the residue that is left after the oil extraction from the seeds. The other precursor employed was the remains of olive wood resulting from the trees prune.
The synthesis of the chemically activated carbons was carried out as described by Solar et al., 2008 following Tsai et al., 1998. The samples were named by taking into account the parameters of synthesis XZnY, where X is the selected raw material; Zn is the activating agent ($ZnCl_2$) and Y, the impregnation relation. The notation for the used raw material (X) comes from their Spanish name: olive lex (Ac), grape lex (Uv) and olive wood (MO).
Carbonized olive lex and olive wood were used for the physical activation. For the samples nomenclature, the raw material was also considered, for example the carbonized olive lex was named LAC and the carbonized olive wood, MOC. The work conditions were described by Solar et al., 2008.
For the textural analysis of the samples, nitrogen adsorption-desorption isotherms were conducted using an AUTOSORB-1MP (Quantachrome Instruments) and an ASAP 2000 (Micromeritics Instruments Corp). Samples were previously degassed at 250°C and the study was carried out at liquid nitrogen temperature, 77K (-196°C). The specific surface was calculated with the Brunauer, Emmet and Teller, BET, method and the pore size distribution by the Density Functional Theory, DFT.
The adsorption analyses of methane were performed using the HPVA100 volumetric equipment (VTI Corp). The apparatus provides isotherms up to 100 bar of pressure at a wide range of temperatures.
Figure 15 shows the adsorption-desorption nitrogen isotherms at 77K for the prepared carbons.

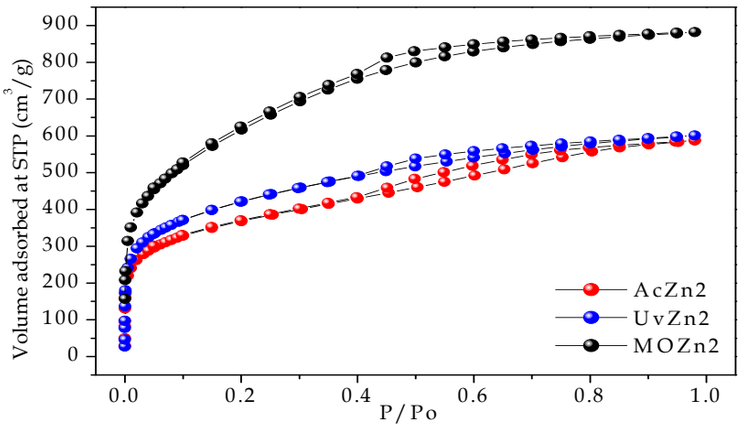

Fig. 15. N_2 adsorption-desorption isotherms obtained from the chemically activated carbons.

The shape of the isotherms is a combination of the Type I at low pressures, characteristic of the microporous solids, and Type IV for higher pressures, according to the Brunauer-Deming-Deming-Teller (BDDT) classification given by Gregg & Sing, 1982. A slight hysteresis loop of the type H2, according to the classification given by Rouquerol et al., 1999 and Martín Martínez, 1990, can be seen, and usually associated to narrow slit-shaped pores.
Table 2 summarizes the data regarding the textural characteristics of the carbons.

Sample	S_{BET} m^2/g	V_T cm^3/g	V_o cm^3/g
AcZn2	1291	0.91	0.54
UvZn2	1470	0.93	0.62
MOZn2	2205	1.36	0.88

Table 2. Textural data from chemically activated carbons.

The specific surface area was calculated by the BET method (S_{BET}) and the micropore volume (V_o) by the Dubinin-Radushkevich method. Finally, the total pore volume (V_T) was estimated from the adsorption of nitrogen at a relative pressure of 0.98 applying the Gurvich rule (Rouquerol et al., 1999). As it can be seen, the sample synthesized from the olive wood is the one showing the better values, that is, higher specific surface area and total volume of pores and micropores.

Figure 16 shows the pore size distribution for the chemically activated samples, where the presence of mesopores can be observed. It was also evidenced by the hysteresis loops of the isotherms. The activated carbon obtained from the olive wood shows a higher quantity of pores, being micro and mesopores. The presence of pores with approximate size of 5Å is more evident for the AcZn2 and UvZn2 samples. The three samples exhibit pores ranging between 10 and 15Å.

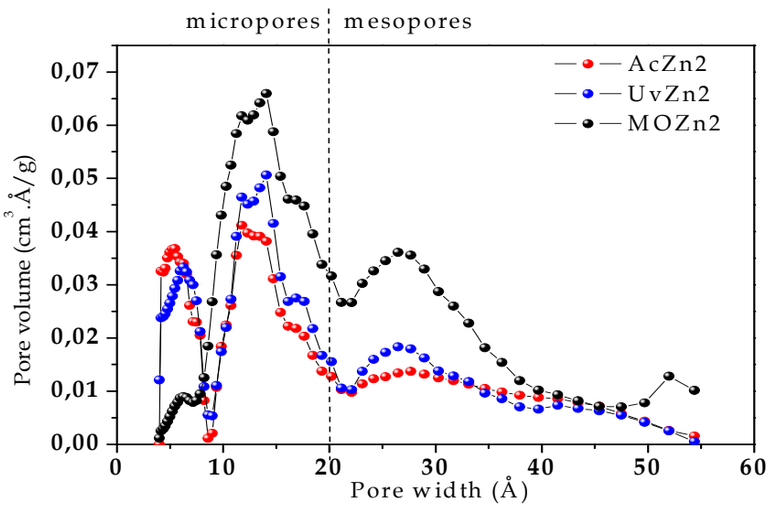

Fig. 16. Pore size distribution (DFT) of the chemically activated carbons.

These materials were assayed in the methane adsorption at high pressure up to 40 bar and at 25°C (Figure 17).

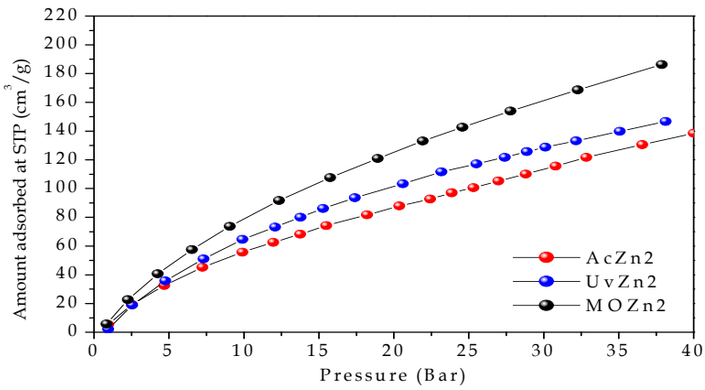

Fig. 17. Methane isotherms from the chemically activated carbons.

Figure 17 shows the isotherms where the samples with higher micropore volumes (Table 2) show higher methane capacity of adsorption in agree with previous reports (Celzard et al., 2005; Lozano-Castelló et al., 2002a; Lozano-Castelló et al., 2002b).
Figure 18 illustrates the isotherms of the physically activated carbon using water vapor. The shape of the isotherms is also a combination of the **Type I** and **IV**, according to the BBDT classification. H2 Hysteresis loops are present.

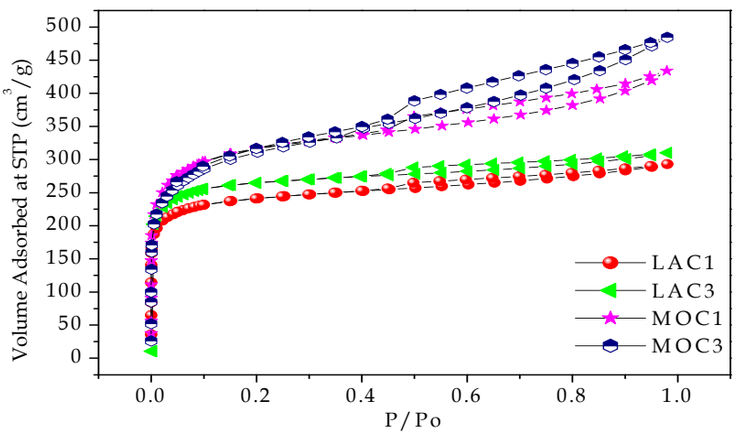

Fig. 18. N_2 adsorption-desorption isotherm from the physically activated carbons.

Table 3 summarizes the textural data from the physically activated carbons using carbonized olive lex (LAC) and carbonized olive wood (MOC) as precursors. By increasing in 30 minutes the activating time for each sample, no significant changes are observed in the specific area, total volume of pores and micropores. Therefore, it seems unnecessary to increase the time by half an hour as the new values are very similar and, at industrial level, the addition of time would increase the costs of the process.

Sample	S_{BET} m^2/g	V_T cm^3/g	V_o cm^3/g	Agent/Material	Temp (°C)	Time (min)
LAC1	913	0.45	0.37	1g/gh	900	120
LAC3	1015	0.48	0.42	1g/gh	900	150
MOC1	1163	0.67	0.48	1g/gh	900	120
MOC3	1117	0.75	0.46	1g/gh	900	150

Table 3. Textural data from the physically activated carbons.

Comparing both set of samples, certain uniformity can be seen related to the specific surface area values, even though the MOC samples show higher values for the total volume of pores and micropores.

Figure 19 illustrates the pore size distribution (DFT) for the physically activated carbons. A similar behavior may be observed between both of them. For the carbons activated from olive lex, it was found that a longer activation time causes the loss of pores smaller than 10Å. However, the time variation applied to the set of activated carbons obtained from olive wood, does not result in a notable change.

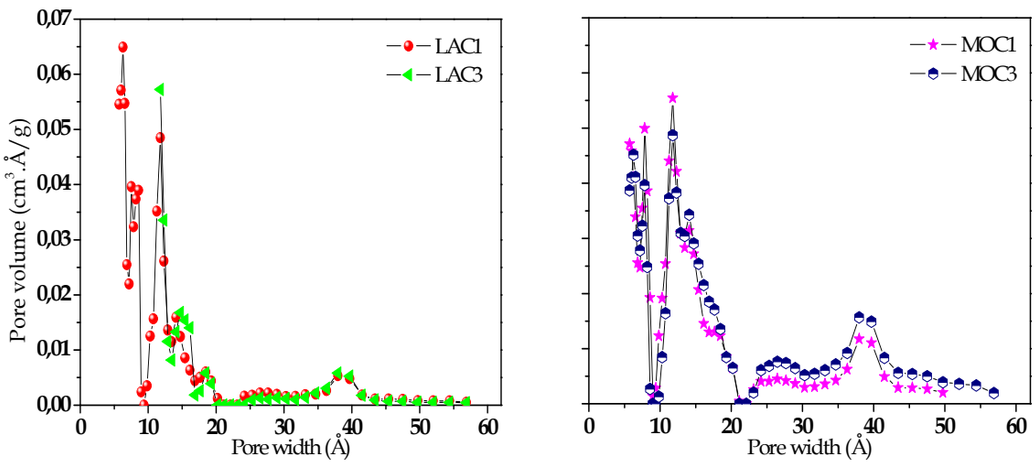

Fig. 19. Pore size distribution (DFT) from the physically activated carbons.

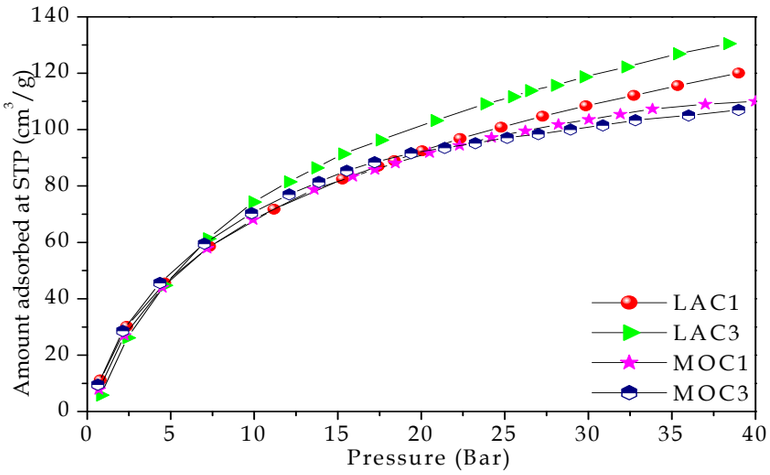

Fig. 20. Methane isotherms from the physically activated carbons.

Regarding the behavior of the physically activated samples in the adsorption of methane, it may be deduced from Figure 20 that they are very similar at low pressures (approximately up to 15 bar). For these samples, a correlation also exists with the nitrogen adsorption that is analogous to the previously observed. However, they show smaller adsorption values than the obtained from the chemically activated samples.

4.2 Monolithic activated carbons

With the aim of increasing the density of the materials and improving their manipulation at technological level, activated carbons in the shape of conglomerates (monoliths) were prepared. Following the methodology described by Almansa et al., 2004, monolithic activated carbons were obtained from coconut shell to study the storage of methane. Figure 21 shows the photographs of the materials.

Fig. 21. Photographs of monolithic activated carbons.

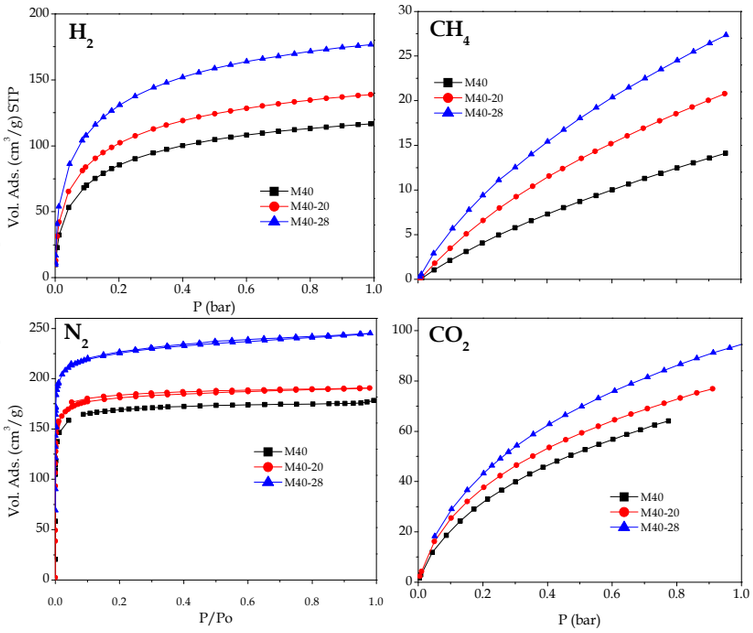

Fig. 22. Adsorption isotherms of N_2 at 77K, H_2 at 77K, CO_2 at 273K and CH_4 at 298K under subatmospheric conditions on the monolithic activated carbons.

The materials were chemically activated with a 40% in weight of $ZnCl_2$ (M40) and subsequently activated using CO_2 to develop higher microporosity up to burn-off percentages of 20 and 28% (M40-20 and M40-28 samples, respectively). For these materials, adsorption isotherms of N_2 at 77K, H_2 at 77K, CO_2 at 273K and CH_4 at 298 K, were measured (Figure 22) at subatmospheric pressures.

From these data, the pore size distribution for each gas was obtained by using a data base of the simulated isotherms through the Monte Carlo method in the Grand Canonical for slit-shaped pores (Figs. 23 to 25). The development of narrow microporosity due to the final activation with CO_2 from the chemically activated monoliths can be observed. Also, the convenience of using various gases for the adequate characterization of the activated carbons becomes evident. The PSDs calculated from the isotherms of CO_2, H_2 and CH_4 can detect narrow porosity that N_2 cannot because, as discussed before, it seems to have diffusion problems. The similitude between the PSDs obtained from CO_2, H_2 and CH_4 at subatmosferic pressures, should be noted (García Blanco et al., 2010).

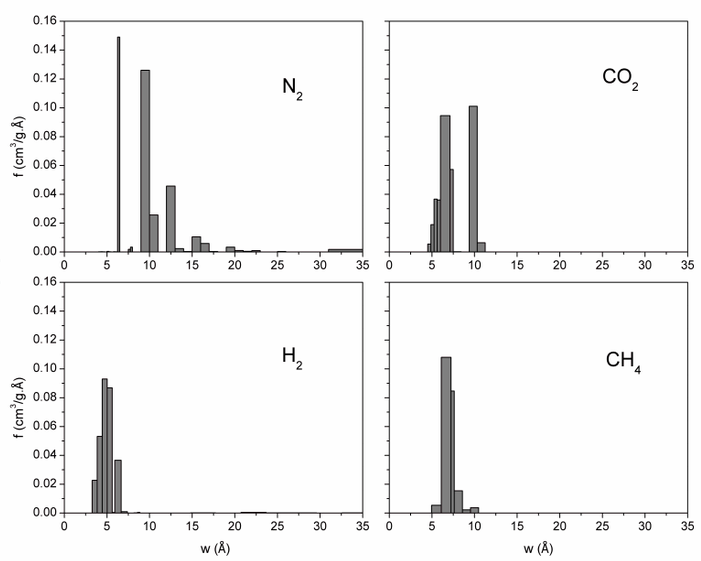

Fig. 23. Pore size distribution from the adsorption isotherms of N_2, H_2, CO_2 and CH_4 for the M40 monolith.

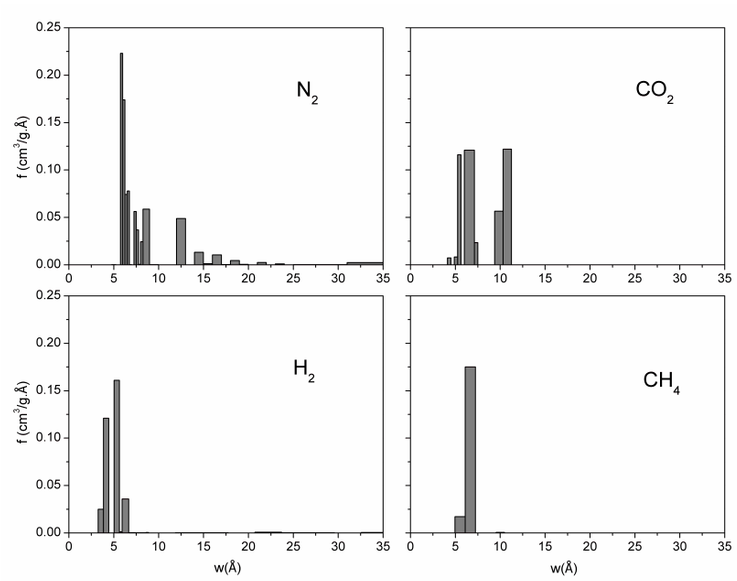

Fig. 24. Pore size distribution from the adsorption isotherms of N_2, H_2, CO_2 and CH_4 for the M40-20 monolith.

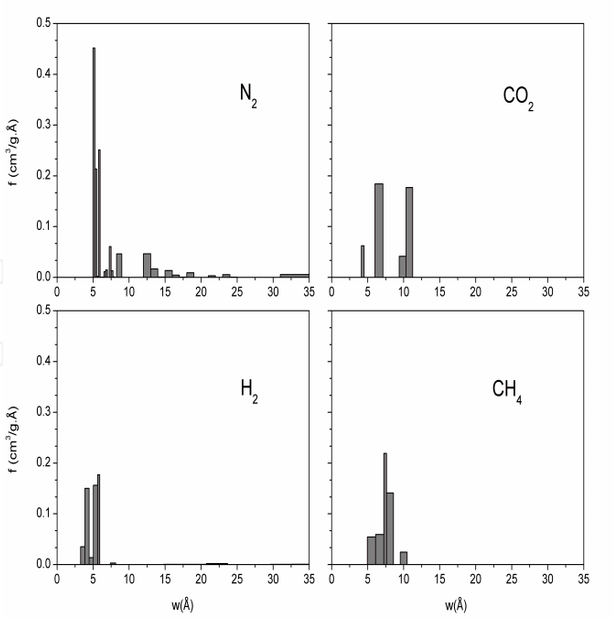

Fig. 25. Pore size distribution from the adsorption isotherms of N_2, H_2, CO_2 and CH_4 for the M40-28 monolith.

Table 4 summarizes the textural data of the samples, comparing diverse methodologies for obtaining the micropore volume. Calculations were made by semi-empirical methods, such as Dubinin-Raduschevich equation and the α-plot method (Gregg & Sing, 1982). The development of the microporosity in the samples and the consistency of the obtained data by the calculated PSDs through Monte Carlo, are remarkable.

	N_2			**CO_2**		**H_2**	**LP-CH_4**
	V_o DR (cm^3/g)	**V_o α-plot (cm^3/g)**	**V_o MC (cm^3/g)**	**V_o DR (cm^3/g)**	**V_o MC (cm^3/g)**	**V_o MC (cm^3/g)**	**V_o MC (cm^3/g)**
M40-0	0.268	0.245	0.259	0.259	0.291	0.175	0.182
M40-20	0.276	0.260	0.291	0.269	0.278	0.204	0.193
M40-28	0.340	0.329	0.378	0.360	0.361	0.269	0.328

Table 4. Textural data of the monolithic activated carbons.

In Figure 26, the adsorption isotherms of CH_4 at 298K and high pressure for the mentioned samples, are shown. The increase in the storage capacity of methane can be seen in accordance to the increase in the microporosity of the samples. This latter was accomplished by the activation with CO_2.

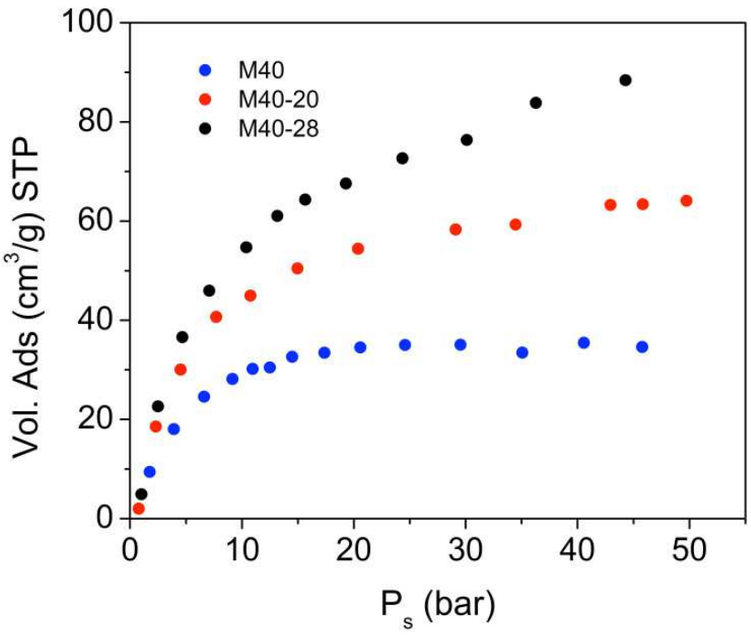

Fig. 26. Methane isotherms from the monolithic activated carbons.

Table 5 present the data obtained for the storage capacity Q', expressed as methane volume stored under STP per stored volume (V/V) calculated at 35 bars with the following equation, given by Celzard et al., 2005:

$$Q' = V / V = Q \cdot M \cdot \mu \cdot \delta ap \tag{23}$$

where Q is the molar storage capacity (mol of methane/kg of activated carbon), M is the molecular weight of methane (g/mol), μ is the volume occupied by 1 gram of methane under STP conditions (1.5dm^3/g) and δap is the apparent density of activated carbon (g/cm^3).

Sample	Ads. Vol. of CH_4 at 35 bar (cm^3/g)	δap (g/cm^3)	V/V
AcZn2	127	0.38	52
UvZn2	129	0.20	28
MOZn2	178	0.30	57
LAC1	115	0.49	60
LAC3	104	0.50	59
MOC1	126	0.18	24
MOC3	98	0.21	23
M40	35	0.80	30
M40-20	60	0.65	42
M40-28	80	0.60	51

Table 5. Methane storage data.

The physically activated samples, called LACs, show improved values of methane storage (approximately 60 v/v) because of its high apparent density. The MOZn2 sample presents higher methane adsorption than LACs but, because of their lower apparent density, they have similar methane storage capacity. Elevated apparent densities can be seen for the monolithic activated carbons. This enhances the storage capacities compared to a sample showing similar textural properties.

4.3 Adsorption of methane on other porous materials

4.3.1 Zeolites and pillared clays (PILCs)

It was studied the adsorption of methane for zeolites (MS-5A and MS-13X with defined pore sizes of 5 Å and 10 Å respectively) and for aluminium pillared clays (PILC Al).
Figure 27 illustrates the isotherms of N_2 at 77K for these materials. As it can be seen, zeolites are strictly microporous materials, showing N_2 adsorption isotherms of Type I. The pillared clay is a micro-mesoporous material (Sapag & Mendioroz, 2001) and the resulting isotherm corresponds to a combination of the Type I and IIb isotherms (Rouquerol et al., 1999). In Table 6, textural properties of the materials calculated from N_2 isotherms, are shown.

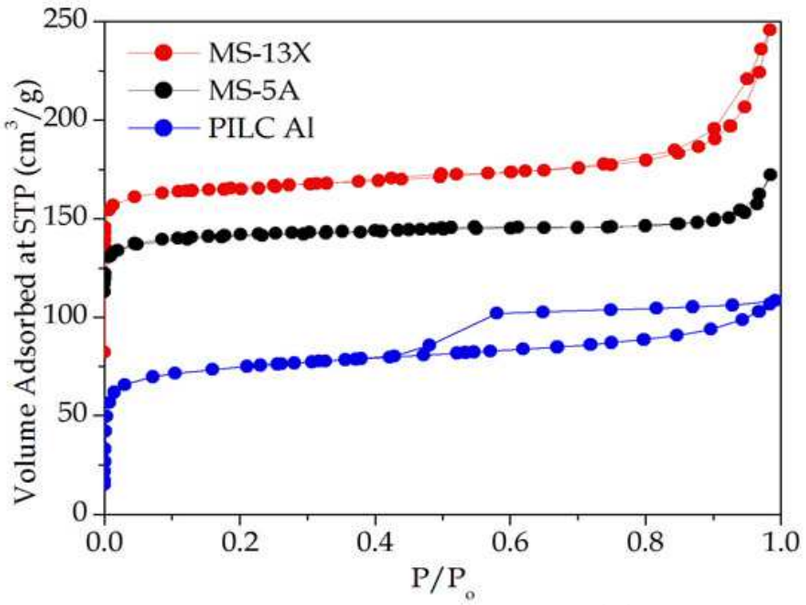

Fig. 27. N_2 adsorption-desorption isotherm for zeolites and PILC.

	S_{BET} (m^2/g)	V_o DR (cm^3/g)	V_T (cm^3/g)
MS-13X	725	0.257	0.320
MS-5A	613	0.221	0.267
PILC Al	283	0.106*	0.170

*Calculated by α-plot

Table 6. Textural data of zeolites and PILC.

In Figure 28 are presented the adsorption isotherms of CH_4 at 298K for zeolites and PILC, at high pressures. For zeolites, the methane adsorption capacity is low due to their pore geometry, among other factors. In addition, the storage capacity of the PILC is particularly low, which is consistent with its lower micropores content in comparison to other materials.

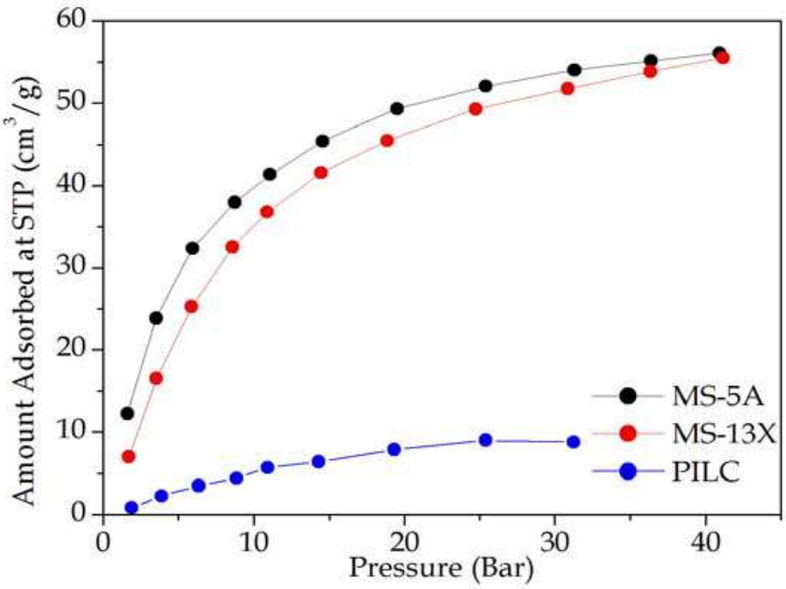

Fig. 28. Methane isotherm for zeolites and PILC.

4.3.2 Carbon nanotubes (NT)

The storage of methane using single-walled carbon nanotubes (SWNT) has been studied. The nanotubes were obtained by chemical vapor deposition (CVD) and commercialized by Carbon Solutions Inc. Since this type of nanotubes usually contain impurities of the catalyst from which they were obtained and from amorphous carbon present with the nanotubes, they are subjected to a purification treatment through the refluxing in concentrated nitric acid (to 65% in weight) at 120°C for 6 hours (NT 6h).

Carbon nanotubes are commonly grouped in bundles of various nanotubes, where the original NT is closed in their end. The treated NT can be opened but they have functional groups at the ends blocking the entrance of the adsorbate molecules (Kuznetsova et al., 2000). Therefore, the adsorption for this kind of materials occur on the IC, G and S sites, indicated in Figure 29, and they have the size of the micropores.

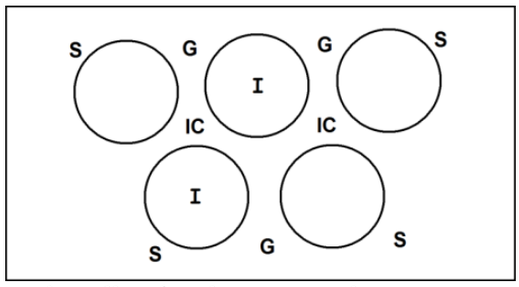

Fig. 29. Adsorption sites in a bundle of carbon nanotubes.

Figure 30 illustrates the N_2 isotherms at 77K of these materials. An important increase in the zone of high relative pressure in the original NT takes place. This is due to the N_2 condensation in the empty sites generated between the nanotubes bundles, corresponding to the meso and macropores. The acid treatment densifies and removes the empty sites (Yang et al., 2005) and the resulting isotherm of the purified nanotubes shows the expected behavior for a microporous material (sites from Figure 29). Table 7 summarizes the textural properties of the materials calculated from the N_2 isotherms.

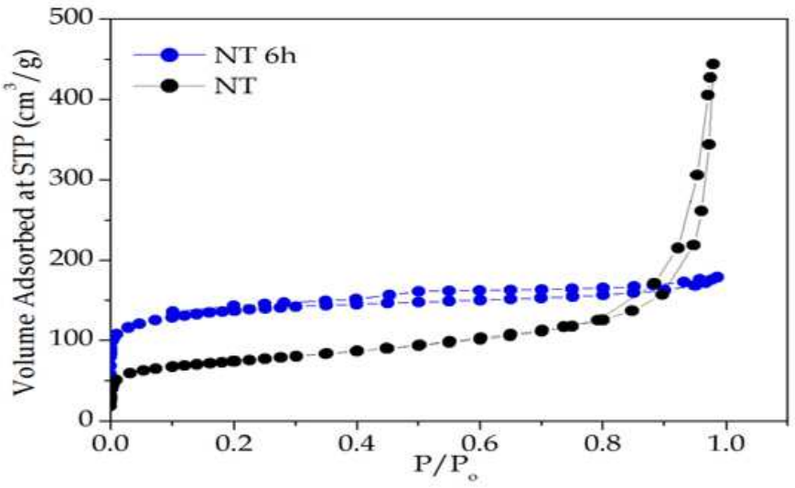

Fig. 30. N_2 adsorption-desorption isotherms of carbon nanotubes.

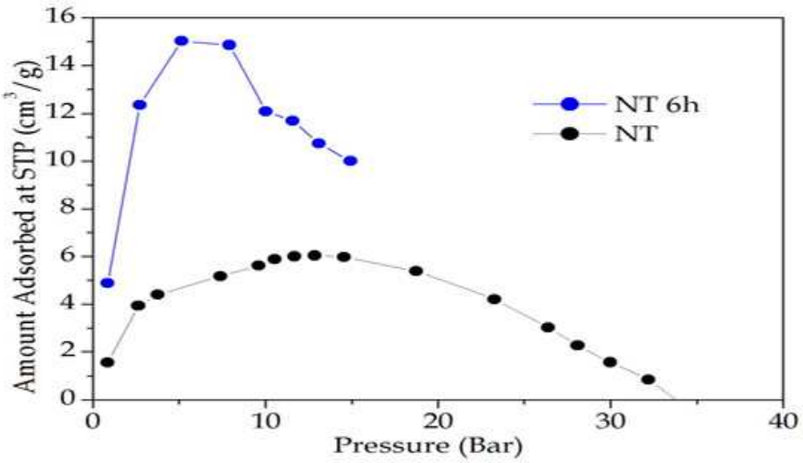

Fig. 31. Methane isotherm of the carbon nanotubes.

	S_{BET} (m^2/g)	V_o DR (cm^3/g)	V_T (cm^3/g)
NT	265	0.11	0.44
NT 6h	510	0.20	0.27

Table 7. Textural data from carbon nanotubes.

Figure 31 corresponds to the CH_4 adsorption at high pressures of the original nanotubes (NT) and the purified nanotubes (NT 6h). For both samples, the CH_4 adsorption is low, indicating that these materials are not suitable for the storage of methane. On the other hand, the decrease in the adsorbed volume along with the pressure increase is due to the saturation of the adsorption sites that are available for methane. Similar observations have been previously reported (Menon, 1968).

4.3.3 Metal Organic Frameworks (MOFs)

The adsorption of methane on MOFs has been studied. MOFs are produced by BASF and commercialized under the denomination of Basolite C300, Basolite A100 and Basolite Z1200. MOFs consist on polymeric framework of metal ions bound one to another by organic ligands. The development during the last few years regarding this type of materials is due to the vast study conducted by the group of Yaghi (Li et al., 1999; Barton et al., 1999). The main characteristics of these materials are the well-arranged pore structure as well as the high pore volume. These features make them attractive for the storage of gases (Lewellyn et al., 2008; Wang et al., 2008; Furukawa & Yaghi, 2009) in spite of their low density.

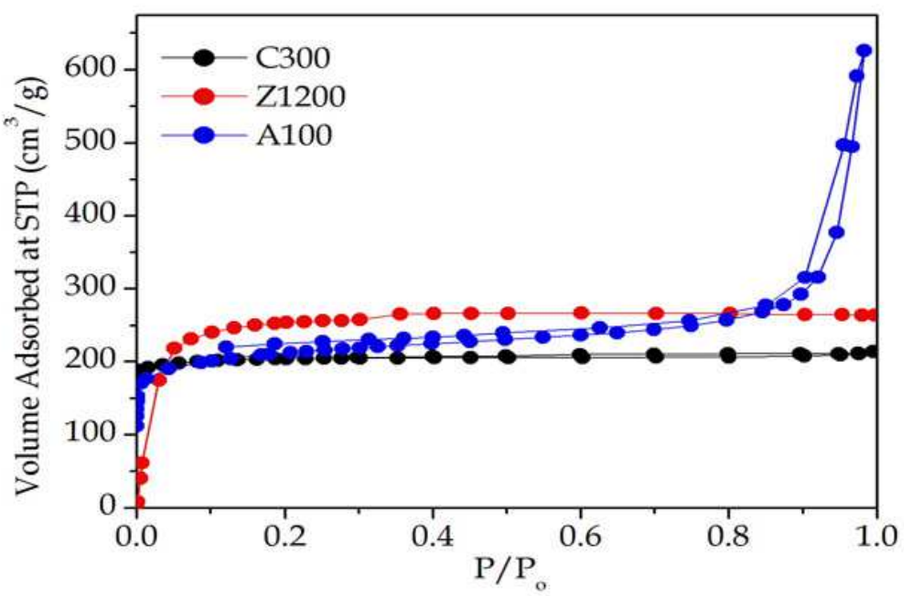

Fig. 32. N_2 adsorption-desorption isotherms of the MOFs.

In Figure 32, an adsorption isotherm of N_2 at 77K for the three studied materials is shown. It is important to note the presence of micropores within the three samples, which is remarked

by the abrupt increase of adsorbed volume at low relative pressures. The isotherms of the C300 and Z1200 samples, present a characteristic plateau of isotherms Type I. In contrast, the growth at high relative pressures of the A100 sample is due to the material flexibility, previously reported by Bourelly et al., 2005.
Table 8 summarizes the data corresponding to the textural characterization of the samples from the N_2 adsorption data, confirming its high microporosity.

	S_{BET} (m^2/g)	V_o DR (cm^3/g)	V_T (cm^3/g)
C300	1059	0.440	0.453
A100	837	0.313	0.969
Z1200	1032	0.421	0.425

Table 8. Textural data of MOFs.

Figure 33 shows the isotherms of CH_4 at 298 K at high pressures. As it can be seen, these samples exhibit a high adsorption capacity for methane, particularly the C300, which almost duplicates the values obtained by the other two samples showing a storage capacity of 70 v/v, evidencing its suitability for the methane storage.
To conclude this chapter, we would like to emphasize the necessity of further research on porous materials, particularly if the purpose of the study is to accomplish the technological application of the ANG process for the storage of methane.

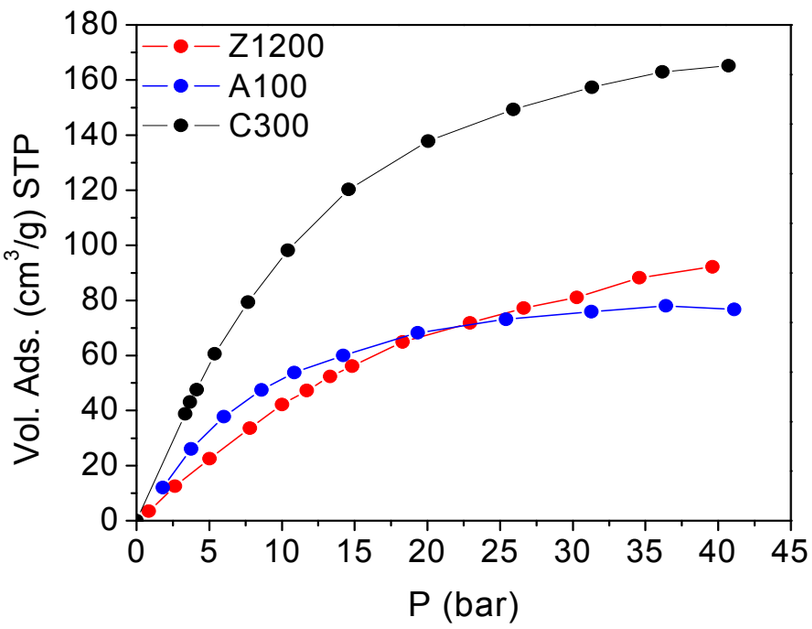

Fig. 33. Methane isotherm for MOFs.

5. Acknowledgements

We want to express our acknowledgement to Universidad Nacional de San Luis, CONICET and FONCyT (Argentine) for the financial support to carry out this work.
Our sincere gratitude to Prof. Aldo Migone, Department of Physics, Southern Illinois University Carbondale, USA, and Prof. Andoni Gil Bravo, Departamento de Química Aplicada, Universidad Pública de Navarra, España for supplying some of the samples reported in this study.

6. References

Alcañiz-Monge, J.; de la Casa-Lillo, M.A.; Cazorla-Amorós, D. & Linares-Solano, A. (1997). Methane storage in activated carbon fibres, *Carbon*, Vol. 35, No. 2, pp. 291-297. ISSN 0008-6223.

Almansa, C.; Molina-Sabio, M. & Rodríguez-Reinoso, F. (2004). Adsorption of methane into ZnCl2-activated carbon derived discs, *Microporous and Mesoporous Materials,* Vol. 76, pp. 185-191. ISSN 1387-1811.

Azevedo, D.C.S.; Rios, R.B.; López R.H.; Torres, A.E.B.; Cavalcante, C.L.; Toso J.P. & Zgrablich G., (2010). Characterization of PSD of activated carbons by using slit and triangular pore geometries. *Applied Surface Science*, Vol. 256, pp. 5191-5197. ISSN 0169-4332.

Barton, T.J.; Buli, L.M.; Klemperer, W.G.; Loy, D.A.; McEnaney, B.; Misono, M.; Monson, P.A.; Pez, G.; Scherer, G.W.; Vartulli, J.C. & Yaghi, O.M. (1999). Tailored porous materials, *Chemistry of Materials*, Vol.11, No.10, pp. 2633-2656. ISSN (electronic): 1089-7690.

Bourelly, S.; Llewellyn, P.L.; Serre, C.; Millange, F.; Loiseau, T & Férey G. (2005). Different adsorption behaviors of methane and carbon dioxide in the isotypic nanoporous metal terephtalates MIL-53 and MIL-47, *Journal the American Chemical Society,* Vol. 127, pp. 13519-13521. ISSN 00027863.

BP Statistical Review of World Energy 2009. (2009). Beyond Petroleum, London. www.bp.com/statisticalreview

Brunauer, S.; Deming, L.S.; Deming, E.W & Teller, E. (1940). On a Theory of the van der Waals Adsorption of Gases, *Journal the American Chemical Society*, Vol. 62, No. 7, pp. 1723-1732. ISSN 00027863.

Brunauer, S.; Emmett, P.H. & Teller, E. (1938). Adsorption of Gases in Multimolecular Layers, *Journal the American Chemical Society*, Vol. 60, No. 2, pp. 309-319. ISSN 00027863.

Celzard, A.; Albiniak, A.; Jasienko-Halat, M.; Mareche, J.F. & Furdin, G. (2005). Methane storage capacities and pore textures of active carbons undergoing mechanical densification, *Carbon,* Vol. 43, pp. 1990-1999. ISSN 0008-6223.

Comisión Nacional de Energía (CNE) (1999). *Información Básica de los Sectores de la Energía*. Edita: CNE, Comisión Nacional de Energía. Publicaciones periódicas anuales. www.cne.es

Cook, T.L.; Komodromos, C.; Quinn, D.F. & Ragan, S. (1999). Adsorbent Storage for Natural Gas Vehicles, In: *Carbon Materials for Advance Technology*, Timothy D. Burchell (Ed.), p. 269-302, Publisher: Pergamon Press Inc, ISBN 0080426832, New York.

Cracknell, R.F.; Gordon, P. & Gubbins, K.E. (1993). Influence of pore geometry on the design of microporous materials for methane storage, *Journal of Physical Chemistry,* Vol. 97, pp. 494-499. ISSN 0022-3654.

Davies, G.M. & Seaton, N.A. (1998). The effect of the choice of pore model on the characterization of the internal structure of microporous carbons using pore size distributions, *Carbon,* Vol. 36, pp. 1473-1490. ISSN 0008-6223.

Davies, G.M. & Seaton, N.A. (1999). Development and validation of pore structure models for adsorption in activated carbons, *Langmuir,* Vol. 15, pp. 6263-6276. ISSN 0743-7463.

Davies, G.M.; Seaton, N.A. & Vassiliadis, V.S. (1999). Calculation of pore size distributions of activated carbons from adsorption isotherms, *Langmuir,* Vol. 15, pp. 8235-8245. ISSN 0743-7463.

Dirección de Tecnología, Seguridad y Eficiencia Energética (2006). *El gas natural vehicular: un combustible con mucho futuro*. http://www.gasnaturalcomercializadora.com

Do, D.D. & Do, H.D. 2003. Adsorption of supercritical fluids in non-porous and porous carbons: analysis of adsorbed phase volume and density. *Carbon*, Vol. 41, No. 9, pp. 1777-1791. ISSN 0008-6223.

Dubinin, D.D. (1960). The Potential Theory of Adsorption of Gases and Vapors for Adsorbents with Energetically Nonuniform Surfaces. *Chemical Reviews*, Vol. 60, No. 2, pp. 235-241. ISSN (electronic) 1520-6890.

Frenkel, D. & Smit, B. (2002). Understanding molecular simulation: From algorithms to applications, Publisher Academic Press, ISBN 0-12-267351, London.

Furukawa, H. & Yaghi, O.M. (2009). Storage of hydrogen, methane, and carbon dioxide in highly porous covalent organic frameworks for clean energy applications, *Journal the American Chemical Society*, Vol. 131, pp. 8875-8883. ISSN 00027863.

García Blanco, A.A.; Alexandre de Oliveira, J.C.; López, R.; Moreno-Piraján, J.C.; Giraldo, L.; Zgrablich, G. & Sapag, K. (2010) A study of the pore size distribution for activated carbon monoliths and their relationship with the storage of methane and hydrogen. *Colloids and Surfaces A: Physicochemical and Engineering Aspects*, Vol. 357, No. 1-3, pp. 74-83. ISSN 0927-7757.

Garrido, J.; Linares-Solano, A.; Martín-Martínez, J. M.; Molina-Sabio, M.; Rodriguez-Reinoso, F. &. Torregrosa, R. (1987). Use of N2 vs. C02 in the Characterization of Activated Carbons, *Langmuir* 1987, Vol. 3, pp. 76-81. ISSN 0743-7463.

Gregg, S.J. & Sing, K.S.W. (1982) *Adsorption, Surface Area and Porosity*. Published Academic Press, ISBN 0123009561, London.

Gubbins, K.E. (1997). Theory and simulation of adsorption in micropores, In: Physical Adsorption: Experiment, theory and applications, Fraissard J. & Conner W.C., (Ed.), pp. 65-103, Kluwer, ISBN 0-7923-4547-9, Dordrecht.

Hill, T.L. (1986). *An Introduction to Statistical Mechanics*, Dover Publications Inc, ISBN 0-486-65242-4, Mineola N.Y.

Inomata, K.; Kanazawa, K.; Urabe, Y.; Hosono, H. & Araki, T. (2002). Natural gas storage in activated carbon pellets without a binder, *Carbon*, Vol. 40, pp. 87-93. ISSN 0008-6223.

Jagiello, J. & Thommes, M. (2004). Comparison of DFT characterization methods based on N2, Ar, CO2 and H2 adsorption applied to carbons with various pore size distributions. *Carbon*, Vol. 42, No. 7, pp. 1227-1232. ISSN 0008-6223.

Jagiello, J.; Ania, C.O.; Parra, J.B.; Jagiello, L.; Pis, J.J. (2007). Using DFT analysis of adsorption data on multiple gases including H2 for the comprehesive characterization of microporous carbons. *Carbon*, Vol. 45, No. 5, pp. 1066-1071 ISSN 0008-6223.

Konstantakou, M.; Steriotis, Th.A.; Papadopoulos, G.K.; Kainourgiakis, M.; Kikkinides, E.S.; & Stubos A.K. (2007). Characterization of nanoporous carbons by combining CO_2 and H2 sorption data with the Monte Carlo simulations. *Applied Surface Science*, Vol. 253, No. 13, pp. 5715-5720. ISSN 0169-4332.

Kuznetsova, A.; Yates, J.T.; Liu, J. & Smalley, R.E. (2000). Physical adsorption of xenon in open single walled carbon nanotubes: Observation of a quasi-one-dimensional confined Xe phase, *Journal of Chemical Physics*, Vol. 112, No. 21, pp. 9590-9598. ISSN (electronic): 1089-7690.

Lastoskie, C.M.; Gubbins, K.E. & Quirke N. (1993). Pore size distribution analysis of microporous carbons : A Density functional approach, *Journal of Physical Chemistry,* Vol. 97, No. 18, pp. 4786-4796. ISSN 0022-3654.

Li, H.; Eddaoudi, M.; O'Keeffe, M. & Yaghi, O.M. (1999) Design and synthesis of an exceptionally stable and highly porous metal-organic framework, *Nature*, Vol. 402, pp. 276-279. ISSN (electronic) 1476-4687.

Llewellyn, P.L.; Bourrelly, S.; Serre, C.; Vimont, A.; Daturi, M.; Hamon, L.; De Weireld. G.; Chang, J.S.; Hong, D.Y.; Hwang, Y.K.; Jhung, S.H. & Férey, G. (2008). High uptakes of CO2 and CH4 in mesoporous metal-organic frameworks MIL-100 and MIL-101, *Langmuir* Vol. 24, pp. 7245-7250. ISSN 0743-7463.

Lozano-Castelló, D.; Alcañiz-Monge, J.; De La Casa-Lillo, M.A.: Cazorla-Amorós, D. & Linares-Solano, A. (2002a). Advances in the study of methane storage in porous carbonaceous materials, *Fuel,* Vol. 81, pp. 1777-1803. ISSN 0016-2361.

Lozano-Castello, D.; Cazorla-Amorós, A.; Linares-Solano, A. & Quinn, D.F. (2002b). Activated carbon monoliths for methane storage: influence of binder, *Carbon* Vol. 40, pp. 2817-2825. ISSN 0008-6223.

Lozano-Castelló, D.; Cazorla-Amorós, D.; Linares-Solano, A. & Quinn, D.F. (2002c). Influence of pore size distribution on methane storage at relatively low pressure: preparation of activated carbon with optimum pore size, *Carbon*, Vol. 40, pp. 989-1002. ISSN 0008-6223.

Lucena, S.M.P.; Paiva, C.A.S.; Silvino, P.F.G.; Azevedo, D.C.S. & Cavalcante Jr., C.L. (2010) The effect of heterogeneity in the randomly etched graphite model for carbon pore size characterization, *Carbon*, Vol. 48, pp. 2554-2565. ISSN 0008-6223.

MacDonald, J.A.F. & Quinn, D.F. (1998). Carbon adsorbents for natural gas storage, *Fuel*, Vol. 77, No. 112, pp. 61-64. ISSN 0016-2361.

Marsh, H. & Rodriguez-Reinoso, F. (2006). *Activated Carbon*. Publisher: Elsevier Science & Technology Books, ISBN 0080444636, Great Britain.

Martín Martínez, J.M. (1990). *Adsorción física de gases y vapores por carbones*, Secretariado de Publicaciones de la Universidad de Alicante (Ed.), Published: Imprenta de la Universidad, ISBN 84-86809-33-9. Universidad de Alicante.

Matranga, K.R.; Myers, A.L. & Glandt, E.D. (1992). Storage of natural gas by adsorption on activated carbon, *Chemical Engineering Science,* Vol. 47, pp. 1569-1579. ISSN 0009-2509.

Menon, P.G. (1968). Adsorption at high pressures, *Chemical Reviews*, Vol. 68, No. 3, pp. 253-373. ISSN (electronic) 1520-6890

Menon, V.C. & Komarnei, S. (1998). Porous adsorbents for vehicular natural gas storage: a review, *Journal of Porous Materials*, Vol. 5, pp. 43-58. ISSN 1380-2224.

Mentasty, L.; Faccio, R.J. & Zgrablich, G. (1991). High Pressure Methane Adsorption in 5A Zeolite and the Nature of Gas-Solid Interactions, *Adsorption Science & Technology*, Vol. 8, pp. 105. ISSN 0263-6174.

Murata, K.; El-Merraoui, M. & Kaneko, K. 2001. A new determination method of absolute adsorption isotherm of supercritical gases under high pressure with a special relevance to density-functional theory study. *Journal of Chemical Physics*, Vol. 114, No. 9, pp. 4196-4205. ISSN (electronic): 1089-7690.

Natural Gas and Climate Change Policy. The European Gas Industry`s View. (1998) EUROGAS, Bélgica. http://www.eurogas.org/publications_environment.aspx

Neimark A.V. & Ravikovitch P.I. (1997). Calibration of pore volume in adsorption experiments and theoretical models, *Langmuir,* Vol. 13, No. 19, pp. 5148-5160. ISSN 0743-7463.

Neimark A.V.; Ravikovitch P.I. & Vishnyakov A. (2000). Adsorption hysteresis in nanopores, *Physical Review E*, Vol 62, No. 2, pp. 1493-1496. ISSN 1550-2376 (online).

Nicholson, D. & Parsonage, N.G. (1982). *Computer simulation and the statistical mechanics of adsorption*, Academic Press, ISBN 0125180608, London.

Parkyns, N.D. & Quinn, D.F. (1995). Natural Gas Adsorbed on Carbon, *Porosity in Carbons*, J. W. Patrick (Ed.), pp. 292-325, ISBN 470-23-454-7, London.

Prauchner, M.J. & Rodríguez-Reinoso, F. (2008). Preparation of granular activated carbons for adsorption of natural gas, *Microporous and Mesoporous Materials*, Vol. 109, pp. 581-584. ISSN: 1387-1811.

Quirke, N. & Tennison, S.R.R. (1996). The interpretation of pore size distributions of microporous carbons. *Carbon*, Vol. 34, No. 10, pp. 1281-1286. ISSN 0008-6223.

Ravikovitch, P. I.; Vishnyakov, A.; Russo, R. & Neimark A.V. (2000). Unified Approach to Pore Size Characterization of Microporous Carbonaceous Materials from N2, Ar, and CO2 Adsorption Isotherms. *Langmuir*, Vol. 16, No. 5, pp. 2311-2320. ISSN 0743-7463.

Rodriguez-Reinoso, F. & Molina-Sabio, M. (1992). Activated carbons from lignocellulosic materials by chemical and/or physical activation: an overview, *Carbon* Vol. 30, No. 7, pp. 1111-1118. ISSN 0008-6223.

Rouquerol, F.; Rouquerol, J. & Sing, K. (1999). *Adsorption by powders and porous solids. Principles, methodology and application,* Published Academic Press, ISBN 0-12-598920-2, London.

Rouquerol, J.; Avnir, D.; Fairbridge, C.W.; Everett, D.H.; Haynes, J.H.; Pernicone, N.; Ramsay, J.D.F.; Sing, K.S.W. & Unger , K.K. (1994). Recommendations For The Characterization Of Porous Solids. *Pure & Applied Chemistry*, Vol. 66, No. 8, pp. 1739-1758. ISSN electronic 1365-3075.

Samios, S.; Stubos, A.K.; Kanellopoulos, N.K.; Cracknell, R.F.; Papadopoulos, G.K. & Nicholson, D. (1997). Determination of micropore size distribution from Gran Canonical Monte Carlo simulations and experimental CO_2 isotherm data. *Langmuir*, Vol. 13, No. 10, pp. 2795-2802. ISSN 0743-7463.

Sapag, K. & Mendioroz, S. (2001). Synthesis and characterization of micro-mesoporous solids: pillared clays, *Colloids and Surfaces A: Physicochemical and Engineering Aspects*, Vol. 187-188, No. 31, pp. 141-149. ISSN 0927-7757.

Scaife, S.; Klusen, P. & Quirke, N. (2000). Characterization of porous materials by gas adsorption: Do different molecular probes give different pore structures?. *Journal of Physical Chemistry B,* Vol. 104, No. 2, pp. 313-318. ISSN (electronic): 1520-5207.

Scaife, S.; Kluson, P. & Quirke, N. (2000), Characterization of porous materials by gas adsorption: Do different molecular probes give different pore structures, *Journal Physical Chemistry B,* Vol. 104, pp. 313-318. ISSN (electronic): 1520-5207.

Sing, K.S.W.; Everett, D.H.; Haul, R.A.W.; Moscou, L.; Pierotti, R.A.; Rouquerol, J. & Siemieniewska, T. (1985). Reporting Physisorption Data For Gas/Solid Systems With Special Reference to the Determination of Surface Area and Porosity, *Pure & Applied Chemistry*, Vol. 57, No. 4, pp. 603-619. ISSN electronic 1365-3075.

Sircar, S.; Golden, T.C. & Rao, M.B. (1996). Activated carbon for gas separation and storage, *Carbon,* Vol. 34, No. 1, p. l-12. ISSN 0008-6223.

Solar, C.; Sardella, F.; Deiana, C.; Montero Lago, R.; Vallone, A. & Sapag, K. (2008). Natural Gas Storage in Microporous Carbon Obtained from Waste of the Olive Oil Production, *Materials Research*, Vol. 11, No. 4, pp. 409-414. ISSN 1516-1439.

Somorjai, G.A. (1994) *Introduction to Surface Chemistry and Catalysis*. John Wiley & Sons, Inc. (Ed.). ISBN: 978-0-471-03192-5, EEUU.

Steele, W.A. 1974. The interaction of gases with solid surfaces, First Edition, Pergamon, ISBN 0080177247, Oxford.

Sun, J.; Brady, T.A.; Rood, M.J.; Lehmann, C.M.; Rostam-Abadi, M. & Lizzio, A.A. (1997). Adsorbed natural gas storage with activated carbons made from Illinois coals and scrap tires, *Energy & Fuels*, Vol. 11, pp. 316-322. ISSN (electronic): 1520-5029.

Sweatman, M.B. & Quirke, N. (2001a). Characterization of porous materials by gas adsorption at ambient temperatures and high pressure, *Journal of Physical Chemistry B,* Vol. 105, pp. 1403-1411. ISSN (electronic): 1520-5207.

Sweatman, M.B. & Quirke, N. (2001b). Characterization of porous materials by gas adsorption: Comparison of nitrogen at 77K and Carbon Dioxide at 298K for activated carbon. *Langmuir*, Vol. 17, No. 16, pp. 5011-5020. ISSN 0743-7463.

Sweatman, M.B. & Quirke, N. (2006). Modelling gas adsorption in slit-pores using Monte Carlo simulation, In: *Adsorption and transport at the nanoscale*, N. Quirke (Ed.) pp. 15-41. CRC Taylor & Francis, ISBN 041532701-6, Boca Raton FL.

Tan, Z. & Gubbins, K.E. (1990). Adsorption in carbon micropores at supercritical temperatures, *Journal of Physical Chemistry,* Vol. 94, pp. 6061-6069. ISSN 0022-3654.

Tarazona P. (1985). Free-energy density functional for hard spheres, *Physical Review A,* Vol. 31, No. 4, pp. 2672-2679. ISSN 1050-2947.

Triebe, R.W.; Tezel, F.H. & Khulbe, K.C. (1996). Adsorption of methane, ethane and ethylene on molecular sieve zeolites, *Gas Separation & Purification,* Vol. 10, Issue 1, pp. 81-84. ISSN 0950-4214.

Wang, B.; Cote, A.P.; Furukawa, H.; O´Keeffe, M. & Yaghi, O.M. (2008). Colosal cages in zeolitic imidazolate frameworks as selective carbon dioxide reservoirs, *Nature* ,Vol. 453, pp. 207-212. ISSN (electronic) 1476-4687.

World Energy Outlook, 2009. Ed: International Energy Agency (IEA), France ISBN: 978-92-64-06130-9. www.iea.org/about/copyright.asp

Yang, C., Kim, D.Y. & Lee, Y.H. (2005). Formation of densely packed single-walled carbon nanotube assembly. *Chemistry of Materials*, Vol.17, pp. 6422-6429. ISSN 0897-4756.

Zhou, L.; Zhou, Y.; Bai, S.; Lü, C. & Yang, B. (2001). Determination of the Adsorbed Phase Volume and Its Application in Isotherm Modeling for the Adsorption of Supercritical Nitrogen on Activated Carbon. *Journal of Colloid and Interface Science*, Vol. 239, No. 1, pp. 33-38. ISSN 0021-9797.

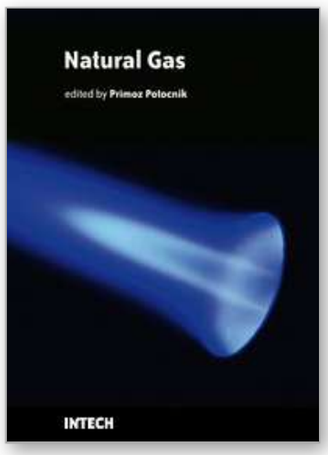

Natural Gas

Edited by PrimoÃ…Â¾ PotoÃ„Ânik

ISBN 978-953-307-112-1
Hard cover, 606 pages
Publisher Sciyo
Published online 18, August, 2010
Published in print edition August, 2010

The contributions in this book present an overview of cutting edge research on natural gas which is a vital component of world's supply of energy. Natural gas is a combustible mixture of hydrocarbon gases, primarily methane but also heavier gaseous hydrocarbons such as ethane, propane and butane. Unlike other fossil fuels, natural gas is clean burning and emits lower levels of potentially harmful by-products into the air. Therefore, it is considered as one of the cleanest, safest, and most useful of all energy sources applied in variety of residential, commercial and industrial fields. The book is organized in 25 chapters that cover various aspects of natural gas research: technology, applications, forecasting, numerical simulations, transport and risk assessment.

InTech Europe
University Campus STeP Ri
Slavka Krautzeka 83/A
51000 Rijeka, Croatia
Phone: +385 (51) 770 447
Fax: +385 (51) 686 166
www.intechopen.com

InTech China
Unit 405, Office Block, Hotel Equatorial Shanghai
No.65, Yan An Road (West), Shanghai, 200040, China
中国上海市延安西路65号上海国际贵都大饭店办公楼405单元
Phone: +86-21-62489820
Fax: +86-21-62489821

IntechOpen